rijksuniversiteit
groningen

Computational Study of Polylactic Acid Synthesis Methods Using *N*-aryl/*N′*-aryl Formazanate Zinc Catalysts

Master of Science thesis

by

Xintao Feng
S2966492

Supervisors

Prof. Dr. Remco Havenith

Prof. Dr. Edwin Otten

Contents

List of Abbreviations

AO	Atomic orbital
ADF	Amsterdam Density Functional
AMS	Amsterdam Modeling Suite
BO	Born-Oppenheimer
COSMO	Conductor-like Screening Model
DFT	Density Functional Theory
DFTB	Density-Functional based Tight-Binding
EDG	Electron-donating group
EWG	Electron-withdrawing group
GGA	Generalized gradient approximation
GHG	Greenhouse gas
IRC	Intrinsic Reaction Coordinate
KS-DFT	Kohn-Sham Density Functional Theory
LDA	Local density approximation
LCAO	Linear combination of atomic orbitals
MO	Molecular orbital
NEB	Nudged Elastic Band
PBE	Perdew-Burke-Ernzerhof
PES	Potential energy surface
PLA	Polylactic acid
QN	quasi-Newton
ROP	Ring opening polymerization
SP	Single Point
SCF	Self-consistent field
TB	Tight-Binding
TST	Transition state theory
TZ2P	Triple-zeta with two polarization functions
XC	Exchange-correlation
ZORA	Zero Order Regular Approximated Hamiltonian

Abstract

Polylactic acid (PLA) is known for its biodegradability and sustainability. In recent years, because of the overuse of petroleum resources leading to excessive greenhouse gas (GHG) emission, the frequent occurrence of extreme weather has increased public concern about protecting the environment. Bioplastics are expected to be an alternative to conventional plastics, reducing the GHGs generated by the using of conventional plastics.

Increasing emphasis is being placed on the concept of using bioplastics to address the growing environmental hazards of the overuse of conventional plastics. This requires advanced synthetic solutions to generate PLA, which may be achieved by ring-opening polymerization (ROP) with *rac*-lactide (rac-LA) as the monomer. This thesis presents a theoretical study for the synthesis of PLA using zinc formazanate complexes that are structurally similar to the well-studied β-diketiminate zinc complexes as redox-active complexes, proposing two reaction mechanisms for the production of PLA as well as establishing three reaction pathways, namely pathways A, B and C, with neutral, radical anionic and radical zinc complexes, respectively.

In this research, a series of computational calculations were carried out using density functional theory (DFT) for ROPs catalyzed by formazanate Zn(II) complexes. These theoretical simulations report the structures of the transition states and intermediates, as well as the Gibbs free energy differences between each state. The calculation results show that: 1) dissociation of a radical anionic dimeric zinc complex tends to produce a neutral and a radical anionic complex; 2) the active species prefers to coordinate with two monomers before starting to polymerize; 3) all three pathways are endothermic with pathway C giving the lowest Gibbs free energy change (ΔG=5.0 kcal/mol); 4) the rate constant of the insertion of another lactide is 0.03 s^{-1}. This study also compared bond distances and free energies calculated by the DFT and DFTB (Density-Functional based Tight-Binding) methods and found that DFTB did not give sufficiently accurate energy predictions in the present calculations. By comparing the free energy changes given by other theoretical calculations and the reaction constants calculated from the experimental data, it was found that the Gibbs free energy difference of pathway C using the radical zinc complex is within a reasonable range of error and has a higher rate constant.

Key words: bioplastics; lactide; polylactide acid; ring-opening polymerization; formazanate ligand; density functional theory; theoretical simulation

Chapter 1 Introduction

1.1 Background

Plastic pollution is a worldwide concern, as it affects the survival of creatures to a large extent, as well as the geographical environment. The annual production of plastics has increased exponentially over the past few decades, with its output increasing by 320.5 million tonnes from 1950 to 2017[1]. Plastics are common to almost all human activities, such as daily life, industrial production and even scientific experiments, because they are particularly convenient and affordable. Most traditional plastics are manufactured using petroleum as an energy resource, which is relatively inexpensive to produce compared to other materials[2]. However, this fossil-based plastic emits large amounts of greenhouse gases (GHGs), and it takes a long time to degrade, which is one reason why it has the potential to influence the geography of the planet[2]. The situation is even worse if there is an unexpected plastic break or chemical reaction during degradation, which is likely to lead to the creation of secondary plastics[3,40]. Considering the time- consuming nature of recycling and degrading petroleum-based plastics, there is an urgent need for human communities to have biodegradable plastic derived from renewable resources.

Polylactic acid (PLA) is a popular non-toxic, recyclable, biocompatible and degradable polymer in the industry that can be derived from the polymerization of lactides[4,5]. Typical uses of PLA are mainly associated with food containers and packing applications, and there is now a growing interest in its potential utilization for tissue engineering and structural applications[6]. Furthermore, due to the unique mechanical properties (e.g. high tensile strength and high modulus properties) and enhanced safety of high-molar mass PLA, its application in 3D printing, microelectronics and science research is a hot topic[7,8]. One of the typical synthetic routes for PLA was established by Carothers[9] in 1932 and is called ring-opening polymerization (ROP), which uses lactic acid and a well-defined metal-based catalyst as reactant and catalyst, respectively. Lactic acid is an environmental friendly monomer as it can be produced through microbial fermentation reactions using organic agricultural waste, kitchen waste and petroleum industry waste as feedstock[3].

1.2 Motivation and Review

A commercially available and efficient synthetic route is urgently needed to satisfy the high demand for PLA from industry and science. Metal complexes with Zn, Mg, Fe, Al, Sn, Ge and Ca as catalytic sites are used in industrial synthesis and academic research on PLA[7,10]. Common synthetic routes for the industrial synthesis of PLA are ROP and

polycondensation (PC), but the synthesis of some of the highly active catalysts used in these routes requires toxic compounds, such as Sn(II) alkoxide[11,12]. Scientists have attempted to find a highly active and non-toxic catalyst system capable of employing lactides for synthesis of PLA. A family of zinc catalysts supported by β-diketiminate ligands is considered by some scientists to be a good candidate[13]. Chellali *et al.* evaluated the influence of different β-diketiminate ligands on the accessibility and stability of the ROP of *rac*-lactide[14]. They showed that the asymmetric zinc complex (*Figure 1.1(a)*) has higher stability and activity and has a TOF value of 13,950 h^{-1} and a M_n value of 7−521 kg/mol. Formazanate ligands are structurally similar to β-diketiminate ligands and offer better flexibility and can also act as redox-active ligands. In this study, zinc formazanate complexes were employed as the active species to catalyst the ROP (*Figure 1.1(b)*).

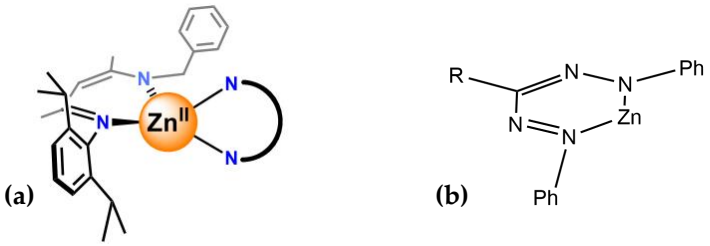

Figure 1.1 The structures of **(a)** β-diketiminate zinc complex[14] and **(b)** formazanate zinc complex.

The formazanate zinc complex behaves as a redox-active substance that can perform the reversible "on−off" switchable catalysis, which allows for the regulation of the ROP process and microstructures[49]. Gregson and co-workers revealed the mechanism of redox-controlled ROP by using a titanium complex with a ferrocenyl-derivatized salen ligand (*Scheme 1.1(a)*)[50]. The chemical redox switch is achieved by tuning the electron density at the Ti atom via the oxidant AgOTf and the reductant Cp*2Fe. The switchable process can be paused, at which point other types of monomers can be added or the synthesis can be ended. This can be applied to other applications, such as the synthesis of biodegradable copolymers[49].

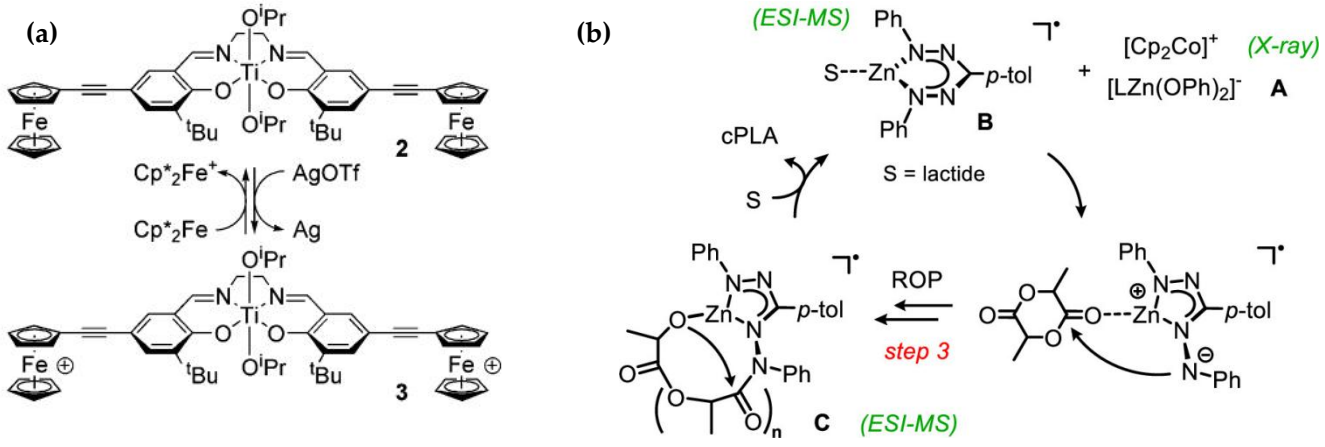

Scheme 1.1 (a) The redox switch of Ti(salen) alkoxide complex[50]. **(b)** Proposed mechanism for cPLA synthesis with formazanate zinc complex[52].

In the research done by De Vries on the ROP of lactide, the formazanate zinc catalyst can process the redox-switch regulation as it has electron donor and acceptor orbitals, and the oxidant and reductant for this regulation are $[Cp_2Fe][PF_6]$ and Cp_2Co, respectively[35,52]. After being reduced by the reducing agent Cp_2Co, the activity of the zinc dimer is turned on, and the subsequent dimer is a radical anion[52]. This experiment uses the radical form of the monomeric zinc complex obtained from the dissociation of the radical anionic zinc dimer to produce cPLA. This experiment provides the basis for the present theoretical research, and the proposed mechanism (*Scheme 1.1(b)*) inspires the postulate that the zinc complex coordinates with two lactides to perform ROP.

1.3 Research Contents

Inspired by studies on β-diketiminate and formazanate ligands, the main content of this research is a computational study based on Density Functional Theory (DFT) to calculate the change in energy during the ROP of lactide to provide a theoretical perspective on this polymerization. The analysis focuses on the dissociation energy of the zinc dimer, the activation energy of the reaction, the Gibbs free energy difference of the elementary steps in ROP and the rate constant of the rate-determining step.

1.3.1 Scientific Questions and Research Aims

The scientific question of this study is to see if the redox-active formazanate zinc complex can catalyze the ROP of lactide with less activation energy by simulating two reaction mechanisms for the synthesis of PLA, and to demonstrate theoretically that the total Gibbs free energy difference is negative, or tends to be negative after more steps, aiming to provide a theoretical basis for the synthesis of PLA using formazanate metal complex as a catalyst. The two mechanisms are: 1) the coordination-insertion mechanism using an active species with one available site; 2) a mechanism using an active species with two available sites. The expected outcome of this study is the discovery of a kinetically favourable pathway for the ROP of lactide using formazanate zinc complexes, providing some theoretical basis for the future synthesis of readily degradable plastics.

1.3.2 Proposed Reaction Mechanisms

Active zinc complexes are obtained by the symmetrical or asymmetrical dissociation of the radical anionic zinc dimers. Two types of reaction mechanisms are simulated in this study. *Scheme 1.2* presents the ROP carried out by the coordination-insertion mechanism. Two transition states appear between the steps from **Int 1** to **Int 2** and the step from **Int 2** to **Int 3**. The polymer in **Int3** is difficult to coordinate with zinc in a cyclic form due to the

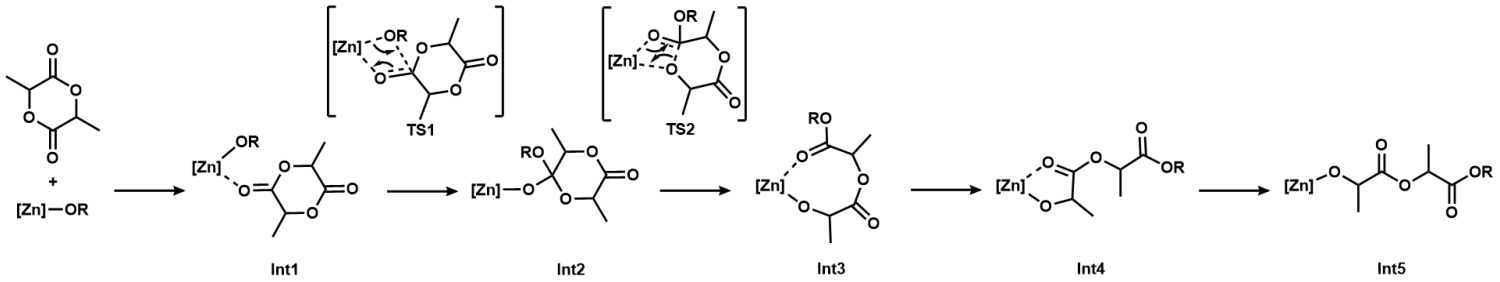

Scheme 1.2 A proposed mechanism[32] with the use of active complexes obtained from the symmetric dissociation. The mechanism is supposed to be the coordination-insertion mechanism.

steric hindrance around the zinc atoms.The polymer then tends to unfold from a ring to a chain, leaving room for the next monomer to coordinate with the zinc atom.

In the other case (*Scheme 1.3*), the active complex obtained by asymmetric dissociation is supposed to have an N in the Zn—N bond capable of attacking the carbonyl carbon in the *rac*-lactide. The rest of the mechanism is similar to the mechanism shown in *Scheme 1.2*. Following a nucleophilic attack by nitrogen on the carbonyl carbon, the first lactide functions similarly to the OR group in the former case. Oxygen next to the carbonyl group undergoes a nucleophilic attack on the carbonyl carbon of the second lactide.

The product appears to be a cyclic PLA (cPLA). It has no chain ends and so has physical and biological properties that differ from its linear form, such as crystallization rate and

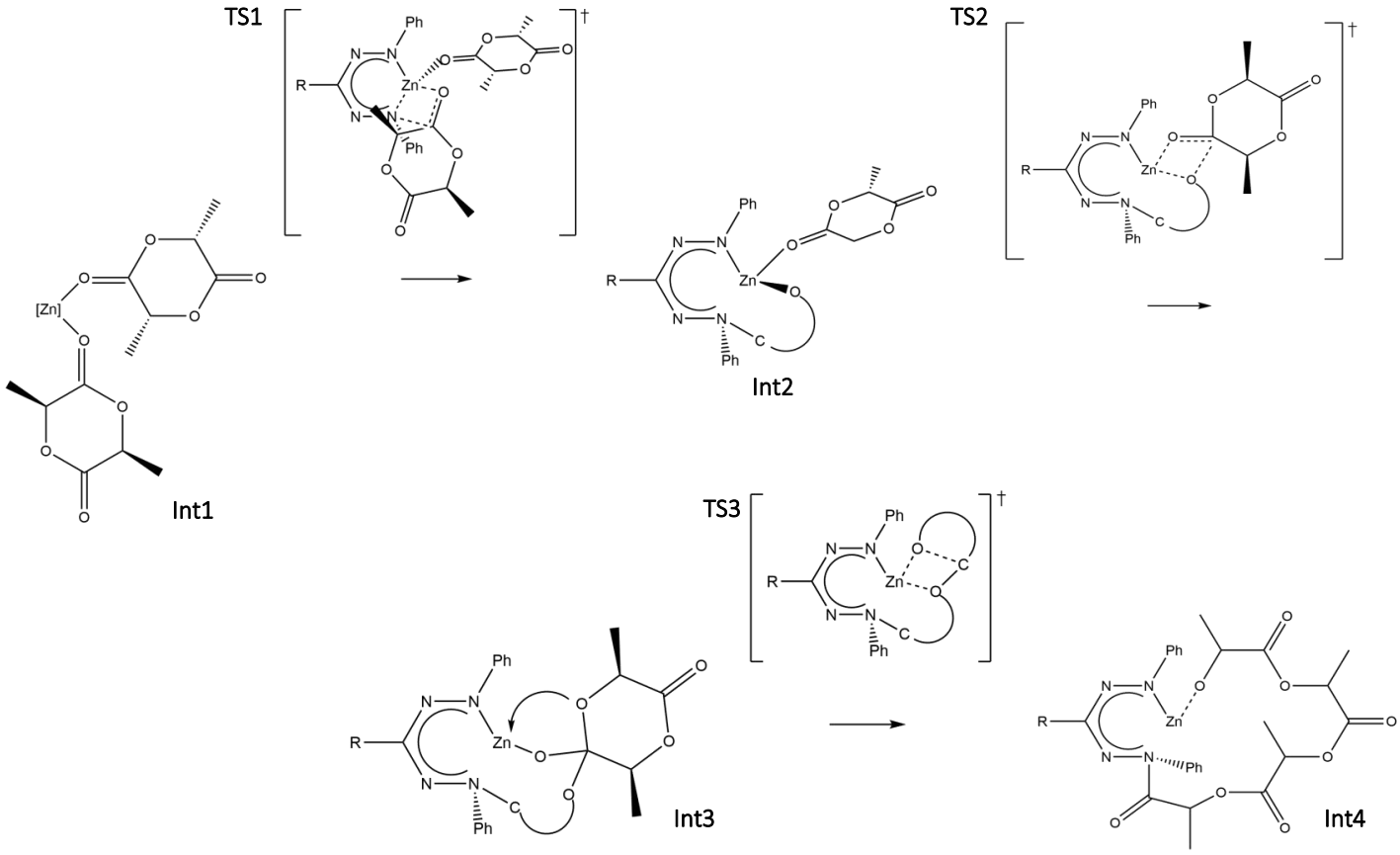

Scheme 1.3 A proposed mechanism with the active complex obtained from the asymmetric dissociation.

the ability of self-assembly[45]. The properties that distinguish cPLA from its linear form are the cyclic topology and the lower intrinsic viscosity. When cPLA degrades, the cleavage of the first ester bond alters the topology from cyclic to linear before the loss of fragments, resulting in a delayed decrease in molecular weight[46,47]. The inherent architecture and thermal stability of cPLA may make it an advanced drug carrier as it may increase the circulation time of polymer gels and improve the thermal stability of micelles[48]. The structure of PLAs are shown in *Figure 1.2(a)* and *(b)*. As cPLA is often obtained as a by-product of its linear form, it is necessary to find a way to synthesize pure cPLA. As shown in *Scheme 1.3* and *Figure 1.2(b)*, the chain ends are coordinated with zinc atoms to maintain the ring structure. This theoretical study attempts to verify that a cPLA with two units can be obtained via pathway C. Further study could be a simulation of subsequent polymerization to see if this mechanism is appropriate for polymerizing a cPLA with more units.

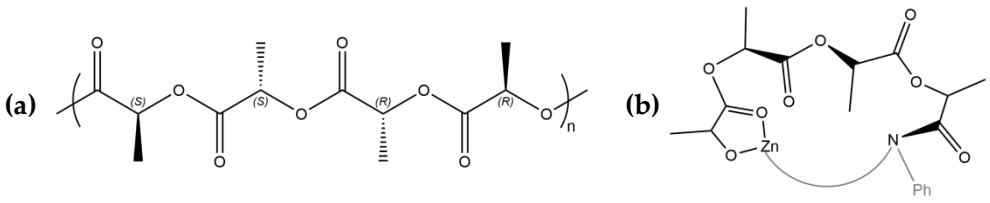

Figure 1.2 The structures of **(a)** linear PLA and **(b)** cyclic PLA with two units.

1.3.3 Computational Tools

The calculations were performed with the Amsterdam Modeling Suite (AMS) program, which uses the Kohn-Sham Density Functional Theory (KS-DFT) method to compute the electronic characteristics of a given system. *Figure 1.3* provides an achievable plan for the construction of the reaction path. The inputs are the molecular structures presented in *Schemes 1.2* and *1.3*. The DFTB method is mainly used to give a preliminary structure and then the DFT method is used to optimize it.

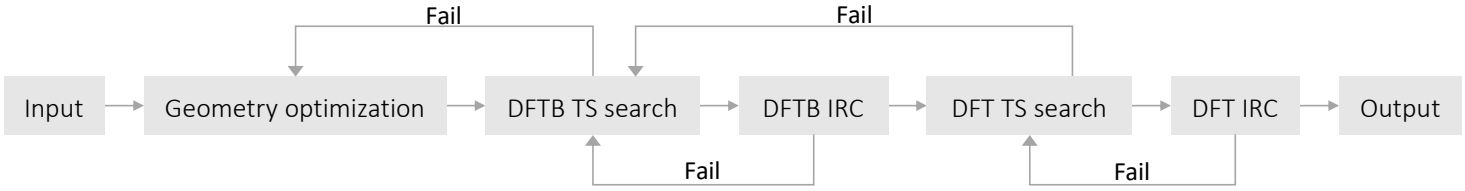

Figure 1.3 General process for finding a transition state.

1.3.4 Implementation Plan

The implementation plan of this research is shown in *Figure 1.4*. The dissociation energy ΔD of dimeric zinc complex is used to determine which dissociation requires the least

energy cost. The Gibbs free energy differences (ΔG) between adjacent states presented in *Schemes 1.2* and *1.3* are used to create energy diagrams for proposed mechanisms, and the ΔG between the rate-determining step and reactant is used to approximate the rate constant k_{rate}. Other ROPs for PLA performed with metal complexes are used to assess whether the errors in this study were within reasonable limits. Furthermore, as the study used the Density-Functional based Tight-Binding (DFTB) method to give the initial structure of each state, the accuracy of the DFTB method is assessed by comparing the bond distances and state energies given by the DFTB and DFT methods.

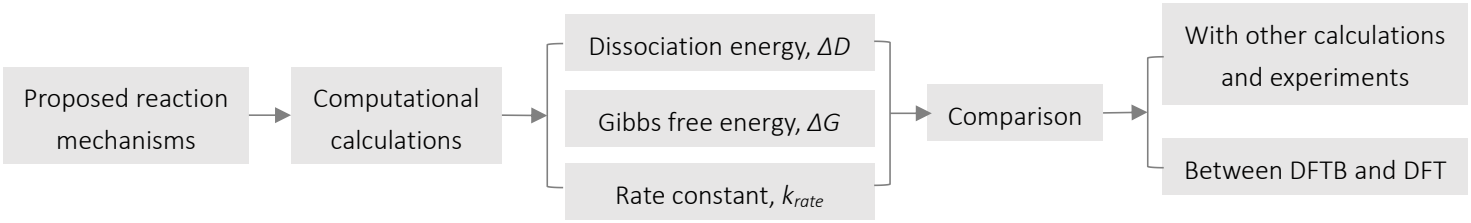

Figure 1.4 Implementation plan of the research.

1.3.5 Highlights of the Study

The zinc dimer with formazanate ligand can dissociate asymmetrically and the resulting active species has an additional position available for coordinating monomers. Also, the formazanate ligand itself has a breakable Zn−N bond, where N can act as a nucleophile. Unlike the coordination-insertion mechanism presented in reactions catalyzed by other β-diketiminate metal complexes, this research postulates a mechanism for a ROP process involving two monomers.

Chapter 2 Theory

Quantum mechanics and its related theories and methods are widely acknowledged and implemented in modern physic and chemistry. In 1926, Schrödinger proposed one of the most famous theories in quantum theory, in which the principal concept is to describe the information of a quantum system with wave functions[21]. The many-body Schrödinger equation is a linear partial differential equation that can be solved using wave function theory or density functional theory (DFT). The latter using the functionals of spatially dependent electron density $\rho(\boldsymbol{r})$ to calculate the molecular electronic structures[22]. The most commonly used DFT utilizes a set of one-electron equations and the Kohn-Sham (KS) theorems to search for a solution to the Schrödinger equation, one of the aims of which is to obtain the total electron energy of a many-body system.

2.1 Basis Set

The molecular orbitals (MOs) can be constructed by combining a set of basis functions describing the electron wave function or electron density. The Slater-type orbital (STO) basis set with the form of exponential functions (*Eq 2.1*) is used to describe MOs.

$$R(r) = Nr^{n-1}e^{-\zeta r} \tag{2.1}$$

In *Eq 2.1* n is the quantum number, N a normalized constant, r the distance between the electron and the nucleus, and ζ is a constant related to the effective charge of the nucleus. The triple-zeta with two polarization (TZ2P) basis set is a core double zeta, valence triple zeta, doubly polarized basis. The additional polarization function has an additional node that provides enough space for electrons to release the repulsive force. A doubly polarized basis has two polarization functions, the second of which has an l value one higher than the l value of the first polarization function. The combination of all AOs constructs the function of MOs (*Eq 2.2*).

$$\psi_i(r) = \sum_{\alpha=1}^{N} c_{\alpha i}\phi_\alpha(r) \tag{2.2}$$

2.2 The Born-Oppenheimer approximation

The Hamiltonian (*Eq 2.3*) for a many-body system with N electrons and M nuclei is:

$$\hat{H} = -\frac{\hbar^2}{2M_i}\sum_{i=1}^{M}\nabla_{R_i}^2 - \frac{\hbar^2}{2m_e}\sum_{i=1}^{N}\nabla_{r_i}^2 + \frac{e^2}{4\pi\varepsilon_0}\left[-\sum_{i=1}^{M}\sum_{j=1}^{N}\frac{Z_i}{\left|\vec{R}_i-\vec{r}_j\right|} + \frac{1}{2}\sum_{j\neq i}^{M}\frac{Z_iZ_j}{\left|\vec{R}_i-\vec{R}_j\right|} + \frac{1}{2}\sum_{j\neq i}^{N}\frac{1}{\left|\vec{r}_i-\vec{r}_j\right|}\right] \tag{2.3}$$

where m_e is the mass of the electron, M_i is the mass of the i^{th} nucleus, $\{r_i\}$ is the position of electron i, $\{R_i\}$ is the position of nucleus i, e is the charge of the electron, and Z_i is the atomic number. The first two terms stand for the kinetic energy of the nuclei and the electrons, while the remaining terms represent the potential energy within the system. The third term is the nucleus-electron attraction, the fourth term is the nucleus-nucleus repulsion, and the last term is the electron-electron repulsion. Using a factor of 1/2 avoids double counting, and using $i \neq j$ avoids counting electrons or nuclei with themselves.

In order to get a reasonable solution to the many-body problem, some approximations to the system are necessary. The first is the Born-Oppenheimer (BO) approximation, which basically states that the extreme mass difference between the electron and the nucleus in the system leads to the nucleus being stationary for the electron so that their motions are separable[23,24]. In other words, the electron motion can be observed without being based on knowledge of the nuclear motion. Given this approximation, the first and fourth terms in *Eq 2.2* can be decoupled from the equation and the electronic Hamiltonian expressed in atomic units constructed from the remaining parts is expressed as *Eq 2.4*.

$$\hat{H}_e = -\frac{1}{2}\sum_{i=1}^{N}\nabla_{r_i}^2 - \sum_{i}^{M}\sum_{j}^{N}\frac{Z_i}{\left|\vec{R}_i - \vec{r}_j\right|} + \frac{1}{2}\sum_{j\neq i}^{N}\frac{1}{\left|\vec{r}_i - \vec{r}_j\right|} \tag{2.4}$$

2.3 Density-Functional Theory (DFT)

The electronic structural properties of a many-body system can be examined by running a series of electronic structure calculations. The Density Functional Theory (DFT) method is a powerful method often used for such calculations, which uses the electronic density as a variable rather than an unknown wave function. Therefore, the electronic property E (i.e., electronic energy) is a functional of the ground state density $\rho(r)$ (*Eq 2.5*).

$$E[\rho(r)] = \int_a^b \rho(r)dr \tag{2.5}$$

In 1927, Llewellyn Thomas and Enrico Fermi first proposed using density functions to solve the Schrödinger equation. In 1930, Paul Dirac improved the functional by adding the exchange energy of the electron to it. Five years later, Carl Friedrich von Weizsacker modified it by introducing a correction term to the kinetic electron energy. In 1964, Pierre Hohenberg and Walter Kohn gave a generalized functional to describe the total electronic energy. Kohn and Lu Jeu Sham further advanced this approach by using a fictitious non-

interacting system with the equivalent electron density as the given system to calculate the electron energy more accurately. Considering these optimizations, the total energy of a given system (*Eq 2.6*) now becomes:

$$E_{tot} = E_T + E_V + E_J + E_X + E_C \tag{2.6}$$

where E_T is the total kinetic energy of the electrons; E_V is the total potential energy of the electron-nucleus attraction; E_J is the total energy of the Coulombic repulsion between the electron pairs; E_X is the total exchange energy of the electrons; E_C is the total correlation energy of the electrons.

2.3.1 Hohenberg-Kohn theorems

Hohenberg and Kohn stated and proved two theorems, the Hohenberg-Kohn theorems, in their first publication on DFT, which are the cornerstones of modern DFT[24].

Theorem 1 For a system of many-body interactions, the external potential $V_{ext}(\vec{r})$ is a unique functional of the ground state electron density $\rho(\vec{r})$.As the Hamiltonian is fixed by $V_{ext}(\vec{r})$, the ground state energy of this system is a unique functional of $\rho(\vec{r})$.

Theorem 2 The functional $E_{HK}[\rho]$, i.e. the functional providing the ground state energy $E[\rho_0]$ of the system, provides the lowest energy if and only if the input electron density is the true ground state electron density ρ_o. It is shown in *Eq 2.7*:

$$E_0 \leq E[\rho_0] = E_T[\rho_0] + E_V[\rho_0] + E_J[\rho_0] \tag{2.7}$$

2.3.2 Exchange-correlation (XC) functional

When the Kohn-Sham formalism is provided to represent the electron kinetic energy, the electron pair Coulombic repulsion energy, and the electron-nuclear attraction energy, the E_X and E_C terms in *Eq. 2.6* are combined into the exchange-correlation functional $E_{XC}[\rho]$. The commonly used exchange-correlation (XC) approximations include the local density approximation (LDA) exchange-correlation functional and the generalized gradient approximation (GGA) exchange-correlation functional. In this study, we apply the latter approach to all calculations[24].

Whether or not the outcomes of the density function method are precise depends largely on the exchange-correlation function applied. In order to make the applications of DFT methods in chemistry and physic more accurate, the charge density gradient $\nabla\rho(\vec{r})$ at the same coordinate has been introduced into the LDA functional (*Eq 2.8*), which enables the

functional to be applied to non-homogeneous systems:

$$E_{XC}^{GGA}\left[\rho_\alpha,\rho_\beta\right]=\int f\left(\rho_\alpha,\rho_\beta,\nabla\rho_\alpha,\nabla\rho_\beta\right)d\vec{r}=E_X^{GGA}+E_C^{GGA} \tag{2.8}$$

The exchange part of the GGA XC functional can be rearranged as in *Eq 2.9*:

$$E_X^{GGA}\left[\rho\right]=E_X^{LDA}\left[\rho\right]-\sum_\sigma\int F\left(s_\sigma\right)\rho_\sigma^{4/3}\left(\vec{r}\right)d\vec{r} \tag{2.9}$$

where $F(s_\sigma)$ is the reduced density gradient for spin σ, which is the functional of the local inhomogeneity parameter s_σ (*Eq 2.10*):

$$s_\sigma\left(\vec{r}\right)=\frac{\left|\nabla\rho_\sigma\left(\vec{r}\right)\right|}{\rho_\sigma^{4/3}\left(\vec{r}\right)} \tag{2.10}$$

In 1996, John P. Perdew, Kieron Burke, and Matthias Ernzerhof (PBE) parameterized the F of E_{XC} to improve further the accuracy of the results[25]. The GGA-PBE functional properly preserves the most vital energy features of the non-local nature of the gradient correction and the correct features of the local electron density. In general, the GGA-PBE functional provides more precise results based on the Kohn-Sham density functional at the position $\vec{r}$ when the electron density $\rho(\vec{r})$ and density gradient $\nabla\rho(\vec{r})$ are introduced, and the final electronic properties are independent of the other positions $\vec{r}'$.

2.4 Tight-Binding (TB) Model

The TB model is applied to various solid-state materials using MOs composed linearly of N local AOs to calculate the electronic band structure, with each AO in use contributing one valence *s*- or *p*-orbital that overlaps only with two immediately adjacent orbitals. The Hamiltonian $h_l(r)$ for the isolated atom l with its nucleus is given by *Eq 3.11*[26]:

$$h_l\varphi_{ml}\left(\boldsymbol{r}-\boldsymbol{r}_{jl}\right)=E_{ml}\varphi_{ml}\left(\boldsymbol{r}-\boldsymbol{r}_{jl}\right) \tag{2.11}$$

where $\boldsymbol{r}_{jl}=\boldsymbol{R}_j+\boldsymbol{r}_l$. The term $\boldsymbol{R}_j$ is the position of jth primitive cell, and r_l is the position of lth atom within the primitive cell. The $\varphi_{ml}\left(r-r_{jl}\right)$term refers to a kind of atomic orbital, namely Löwdin orbital. Such atomic wave functions are confined to different atoms and are orthogonal to each other. Considering the translational symmetry of a periodic crystal, the unperturbed wave functions will be *Eq 3.12*[26]:

$$\Phi_{mlk}=\frac{1}{\sqrt{N}}\sum_i\exp\left(i\boldsymbol{r}_{jl}\cdot\boldsymbol{k}\right)\phi_{ml}\left(\boldsymbol{r}-\boldsymbol{r}_{jl}\right) \tag{2.12}$$

where m refers to the m-th atomic energy level. The TB model is not sufficiently accurate

due to the lack of explicit basic functions. As a result, TB eigenstates and explicit basis functions may not be compatible, potentially leading to further incorrect calculations or predictions of physical properties[27].

2.5 Density-Functional based Tight-Binding (DFTB) Method

The DFTB method gives an approximate DFT calculation for a given electronic structure and gives a first insight into the electronic properties of the interacting electronic system. Fast calculation with the DFTB method is an inexpensive and effective way to optimize the input electronic structure for DFT calculation by using the optimal DFTB molecular geometry as the import coordinate for DFT.

The DFTB method can also be described as an approximate quantum chemistry method when the idea of Kohn-Sham DFT is introduced, where the electron density can be written in the form of Kohn-Sham orbitals. These orbitals φ_i are described by the linear combination of atomic orbitals (LCAO) method, which presents the one-electron function in terms of a superposition of atomic wave functions (*Eq 2.13*)[28]:

$$\varphi_i(\vec{r}) = \sum_{\nu}^{N} C_{i\nu}\phi_\nu\left(\vec{r} - \vec{R}_\alpha\right) \tag{2.13}$$

where ϕ_ν is the basis function, $C_{i\nu}$ is the expansion coefficient, and R_α is the position of the isolated atom. In order to make the DFTB more accurate, some supplements are added to the total energy expression. By introducing the second-order term in density fluctuations, the resulting self-consistent charge DFTB (SCC-DFTB) model is able to provide the total energy of the intermediate charge transfer (*Eq 2.14*)[29]:

$$E_{tot}^{SCC-DFTB} = E_{H_0} + E_\gamma + E_{rep} \tag{2.14}$$

where E_0 represents the total energy contributed by the reference electron density ρ_0 and E_{rep} is the contribution from repulsive interaction, including the nuclear-nuclear repulsion and the electron-electron repulsion. The second term E_γ, is an approximate second-order term for the DFTB total energy which takes into account the effect of intermediate charge transfer and assumes a spherical electron density.

2.6 Mathematics of Transition State

The mathematical approach to identifying whether a PES point representing molecular geometry in computational chemistry is a local minimum or a saddle point is to look at the gradient and curvature of the point. The first partial derivative of a point stands for

the gradient and the point is defined as a stationary point when its value is zero (*Eq 2.15*).

$$\left(\frac{\partial E}{\partial R}\right) = 0 \tag{2.15}$$

The second partial derivative of the stationary point represents the curvature and the rate of change of energy in a particular direction. The curvature of the lowest point is positive in all directions; the curvature of the saddle point is negative in one or more directions and positive in the others (*Eq 2.16*):

$$\left(\frac{\partial^2 E}{\partial R_{para}^2}\right) < 0\,, \quad \left(\frac{\partial^2 E}{\partial R_{perp}^2}\right) > 0 \tag{2.16}$$

where R_{para} refers to the direction parallel to the reaction coordinate, and R_{perp} refers to the direction perpendicular to the reaction coordinate. A positive value of curvature implies an increase in energy, while a negative value implies a decrease in energy. The transition state on the PES is located at a saddle point, as shown in *Figure 2.1*.

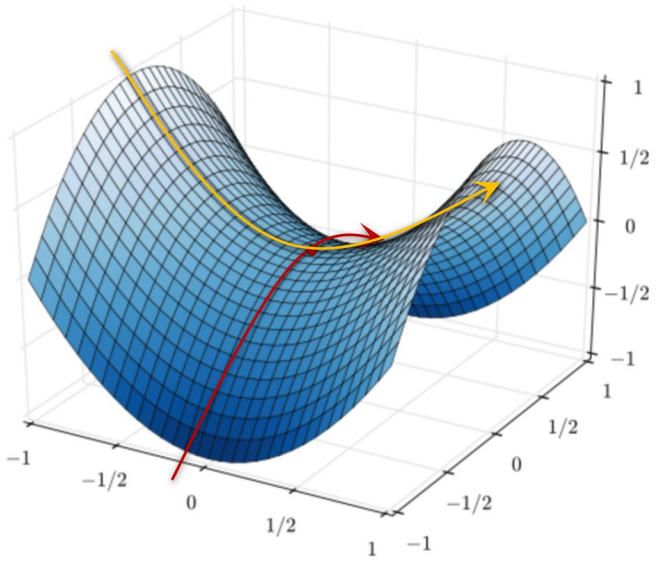

Figure 2.1 The saddle point is the intersection of the red and yellow curves on the PES-like surface. The red curve represents the reaction coordinate whereas the yellow curve represents the direction perpendicular to the reaction coordinate.

2.7 Vibrational Frequency and IR intensity

The second-order partial derivatives of a PES point form the Hessian matrix whose eigenvectors are the normal modes and whose eigenvalues are related to frequencies. The Hessian matrix includes the curvature of a PES point in *x*-, *y*- and *z*-directions (*Eq 2.17*). The positions are (x_1, y_1, z_1), (x_2, y_2, z_2), ... , (x_n, y_n, z_n).

$$H_E = \begin{bmatrix} \frac{\partial^2 E}{\partial x_1^2} & \frac{\partial^2 E}{\partial x_1 \partial y_1} & \frac{\partial^2 E}{\partial x_1 \partial z_1} & \frac{\partial^2 E}{\partial x_1 \partial x_2} & \frac{\partial^2 E}{\partial x_1 \partial y_2} & \frac{\partial^2 E}{\partial x_1 \partial z_2} & & \frac{\partial^2 E}{\partial x_1 \partial x_n} & \frac{\partial^2 E}{\partial x_1 \partial y_n} & \frac{\partial^2 E}{\partial x_1 \partial z_n} \\ \frac{\partial^2 E}{\partial y_1 \partial x_1} & \frac{\partial^2 E}{\partial y_1^2} & \frac{\partial^2 E}{\partial y_1 \partial z_1} & \frac{\partial^2 E}{\partial y_1 \partial x_2} & \frac{\partial^2 E}{\partial y_1 \partial y_2} & \frac{\partial^2 E}{\partial y_1 \partial z_2} & \cdots & \frac{\partial^2 E}{\partial y_1 \partial x_n} & \frac{\partial^2 E}{\partial y_1 \partial y_n} & \frac{\partial^2 E}{\partial y_1 \partial z_n} \\ \frac{\partial^2 E}{\partial z_1 \partial x_1} & \frac{\partial^2 E}{\partial z_1 \partial y_1} & \frac{\partial^2 E}{\partial z_1^2} & \frac{\partial^2 E}{\partial z_1 \partial x_2} & \frac{\partial^2 E}{\partial z_1 \partial y_2} & \frac{\partial^2 E}{\partial z_1 \partial z_2} & & \frac{\partial^2 E}{\partial z_1 \partial x_n} & \frac{\partial^2 E}{\partial z_1 \partial y_n} & \frac{\partial^2 E}{\partial z_1 \partial z_n} \\ \frac{\partial^2 E}{\partial x_2 \partial x_1} & \frac{\partial^2 E}{\partial x_2 \partial y_1} & \frac{\partial^2 E}{\partial x_2 \partial z_1} & \frac{\partial^2 E}{\partial x_2^2} & \frac{\partial^2 E}{\partial x_2 \partial y_2} & \frac{\partial^2 E}{\partial x_2 \partial z_2} & & \frac{\partial^2 E}{\partial x_2 \partial x_n} & \frac{\partial^2 E}{\partial x_2 \partial y_n} & \frac{\partial^2 E}{\partial x_2 \partial z_n} \\ \frac{\partial^2 E}{\partial y_2 \partial x_1} & \frac{\partial^2 E}{\partial y_2 \partial y_1} & \frac{\partial^2 E}{\partial y_2 \partial z_1} & \frac{\partial^2 E}{\partial y_2 \partial x_2} & \frac{\partial^2 E}{\partial y_2^2} & \frac{\partial^2 E}{\partial y_2 \partial z_2} & \cdots & \frac{\partial^2 E}{\partial y_2 \partial x_n} & \frac{\partial^2 E}{\partial y_2 \partial y_n} & \frac{\partial^2 E}{\partial y_2 \partial z_n} \\ \frac{\partial^2 E}{\partial z_2 \partial x_1} & \frac{\partial^2 E}{\partial z_2 \partial y_1} & \frac{\partial^2 E}{\partial z_2 \partial z_1} & \frac{\partial^2 E}{\partial z_2 \partial x_2} & \frac{\partial^2 E}{\partial z_2 \partial y_2} & \frac{\partial^2 E}{\partial z_2^2} & & \frac{\partial^2 E}{\partial z_2 \partial x_n} & \frac{\partial^2 E}{\partial z_2 \partial y_n} & \frac{\partial^2 E}{\partial z_2 \partial z_n} \\ & \vdots & & & \vdots & & \ddots & & \vdots & \\ \frac{\partial^2 E}{\partial x_n \partial x_1} & \frac{\partial^2 E}{\partial x_n \partial y_1} & \frac{\partial^2 E}{\partial x_n \partial z_1} & \frac{\partial^2 E}{\partial x_n \partial x_2} & \frac{\partial^2 E}{\partial x_n \partial y_2} & \frac{\partial^2 E}{\partial x_n \partial z_2} & & \frac{\partial^2 E}{\partial x_n^2} & \frac{\partial^2 E}{\partial x_n \partial y_n} & \frac{\partial^2 E}{\partial x_n \partial z_n} \\ \frac{\partial^2 E}{\partial y_n \partial x_1} & \frac{\partial^2 E}{\partial y_n \partial y_1} & \frac{\partial^2 E}{\partial y_n \partial z_1} & \frac{\partial^2 E}{\partial y_n \partial x_2} & \frac{\partial^2 E}{\partial y_n \partial y_2} & \frac{\partial^2 E}{\partial y_n \partial z_2} & \cdots & \frac{\partial^2 E}{\partial y_n \partial x_n} & \frac{\partial^2 E}{\partial y_n^2} & \frac{\partial^2 E}{\partial y_n \partial z_n} \\ \frac{\partial^2 E}{\partial z_n \partial x_1} & \frac{\partial^2 E}{\partial z_n \partial y_1} & \frac{\partial^2 E}{\partial z_n \partial z_1} & \frac{\partial^2 E}{\partial z_n \partial x_2} & \frac{\partial^2 E}{\partial z_n \partial y_2} & \frac{\partial^2 E}{\partial z_n \partial z_2} & & \frac{\partial^2 E}{\partial z_n \partial x_n} & \frac{\partial^2 E}{\partial z_n \partial y_n} & \frac{\partial^2 E}{\partial z_n^2} \end{bmatrix} \quad (2.17)$$

where E is the energy of a PES point; x, y and z stand for the x-, y- and z- components of the point on PES. The Hessian can be analytically calculated for a GGA-PBE functional with AMS.

2.8 Rate constant

The rate constant k_{rate} for an elementary step is given by *Eq 2.18*[54], which uses the idea of transition state theory (TST), considering the TS as an equilibrium state of the reactant.

$$k_{rate} = \frac{kT}{h} \exp[-\Delta G^{\neq}/RT] \quad (2.18)$$
$$\Delta G^{\neq} = G_{\mathrm{TS}} - G_{\mathrm{reactant}}$$

The coefficient including Boltzmann's constant k_B, Planck constant h and temperature T. Term $\Delta G^{\neq}$ is the Gibbs free energy difference between transition state and reactant.

Chapter 3 Methods

Based on the results of previous research mentioned in Chapter 1, reaction mechanisms of the two types of pathways can be drafted. An elementary step consists of a transition state and two adjacent intermediates. The AMS allows the construction of the coordinates of the catalytic system and the calculation of the energy of a given system at the level of GGA-PBE/TZ2P including scalar relativistic effects using ZORA[30]. The size of frozen core is set to small and the numerical quality is set to normal. The method used to investigate solvent effects was the Conductor-like Screening Model (COSMO) with dichloromethane (DCM, CH_2Cl_2) as the solvent and the Allinger radii as the default atomic radii[31]. The DFTB calculation gives an approximate result, and the DFT calculation improves the resulting geometry further.

3.1 Geometry Optimization

The purpose of geometry optimization is to reduce the total energy of the given system by modifying its geometry, which usually locates at a local minimum on the PES[33]. The optimization algorithm is selected automatically by the AMS program. The ADF engine is moderate and slow, so the quasi- Newton (QN) optimizer is an appropriate choice for searching the transition state[33]. It uses the QN method and is able to search for the local minimum geometry from the current point[31]. The threshold value for nuclear gradients is 0.001 Hartree/Å; the criterion value for energy change is 10^{-05} Hartree. The maximum Cartesian step for a converging geometry is 0.01 Å. There is no limit on the maximum number of iterations given for this calculation.

3.2 Transition State Search

The Task Transition State Search of the AMS program performs operations similar to the geometry optimization and gives information on frequency and IR intensity[33]. Similarly, the gradient convergence, energy convergence and step convergence are set to 0.001 Hartree/Å, 10^{-05} Hartree and 0.01 Å. The input geometry may need manual adjustment as the lower harmonicity of the PES close to the TS makes it harder for the QN optimizer to find the stationary point. This situation can be resolved by using the initial Hessian obtained from the DFTB calculation with the file extension *.rkf*.

3.3 Single Point Calculation

The PES point properties of a hypothetical transition state can be quickly viewed by the Task Single Point. It provides information on the properties of the PES point, including

gradients, normal mode frequencies, charges, spin population, orbital occupations and orbital degeneracies[33]. The information can be checked directly through the output file.

3.4 Intrinsic Reaction Coordinate (IRC) Method

The IRC calculation tracks the geometry of the reactants and products connected to the transition state. The forward and backward directions are determined by the sign of the maximum component of the vibrational normal mode of the transition state geometry, the signs being positive and negative respectively[33].

The forward and backward directions are calculated alternatively, which means that the program will calculate the forward path first and then the backward one[33]. The result of the previous TS search is employed to be the initial Hessian for the corresponding IRC calculation. The maximum iterations are 300, and the maximum number of points are 100. The gradient convergence is 10^{-3} Hartree/Å and the step convergence is 10^{-3} Å. The step size is 0.2 sqrt(amu)*bohr. Each IRC endpoint is optimized with the same setting as the geometry optimization. The converged results are preserved when we need to check the information on binary RKF results (e.g. forward path and backward path).

3.5 DFTB Calculation

A fast approximate calculation of the transition state in each elementary step was carried out using the Density-Functional based Tight-Binding (DFTB) method before the energy of the transition state was calculated using the DFT method. The geometries of initial and final states were optimized to construct a possible reaction pathway. A transition state to be determined is established based on the change in the bond between two neighbouring intermediates. The Nudged Elastic Band (NEB) method constructs a rough reaction path along a given set of molecular structures. The structure with the highest energy is used for the transition state task running by DFTB engine. The initial model Hessian is picked automatically by the program when optimizing the geometry.

The Hamiltonian used in DFTB method is SCC-DFTB, which includes a self-consistency loop for Mulliken charges. The orbitals are filled automatically by the program with the strategy to fill the lowest energy orbitals with paired or unpaired electrons[33]. The DFTB parameters directory is DFTB.org/auorg-0-1.

A structure with a negative vibrational frequency and close to or above 100 cm^{-1} is used to perform the Single Point calculation and then its gradient and frequency are examined to determine if the geometry lies at a stationary point on the PES. The IRC calculation is run on it to estimate whether this transition state (e.g. stationary point) will lead to the

desired reactant and product. The Single Point calculation should give zero gradients and the IRC calculation should display the adjacent intermediates given in the proposed mechanisms. Once the geometry has successfully passed the proper checks for Single Point and IRC calculations, it can be used for further DFT calculations.

3.5.1 Nudged Elastic Band (NEB) Method

The NEB method is employed in the DFTB calculation step. It enables the construction of a possible reaction pathway based on two or three given geometries and displays the pathway using a set of images[33]. The number of images is eight; the maximum number of iterations depend on the number of images and atoms. The spring force constant is 1.0 Hartree/Bohr^2; the skewness is set to 1.0. The geometry of initial images are obtained by interpolation in internal coordinates between the given reactants and products. The given geometry would be optimized automatically when the calculation start, which used the default condition given by the program.

3.6 DFT Calculation

The DFT calculations were performed using the PBE exchange-correlation functional. The TZ2P basis set was selected in order to give a result with relatively good quality. Scalar relativistic effects at Zero Order Regular Approximated Hamiltonian (ZORA) formalism, and the nuclear charge distribution was simulated by a Point Charge model[33]. The small-size frozen core was selected. The level of numerical quality was set to normal.

Chapter 4 Results and Discussions

4.1 Properties of the formazanate Zn(II) complex

Formazanate ligands are structurally similar to β-diketiminate ligands, which are widely used in *rac*-lactide (*rac*-LA) ring-opening polymerization (ROP). The formazanate Zn(II) complex has a redox-active ligand with a high level of structural flexibility, allowing it to be compatible with steric hindrance[35]. The $Ar^1-N=N-C=N-NH-Ar^5$ backbone contains four nitrogen atoms and can form a six- or five- membered chelate ring by isomerization. The bond lengths of the $N-C$ and $N=N$ bonds are about 1.34 Å. The formazanate Zn(II) complexes are likely to have a six-membered chelate ring when the electronic properties of the Ar^1 and Ar^5 substitutes are similar[35]. Zinc dimers **1** and **4** shown in *Scheme 4.1(a)* and *(b)* are radical anions and are the products of reduction reactions with, for example, Cp_2Co or Na/Hg reducing agent.

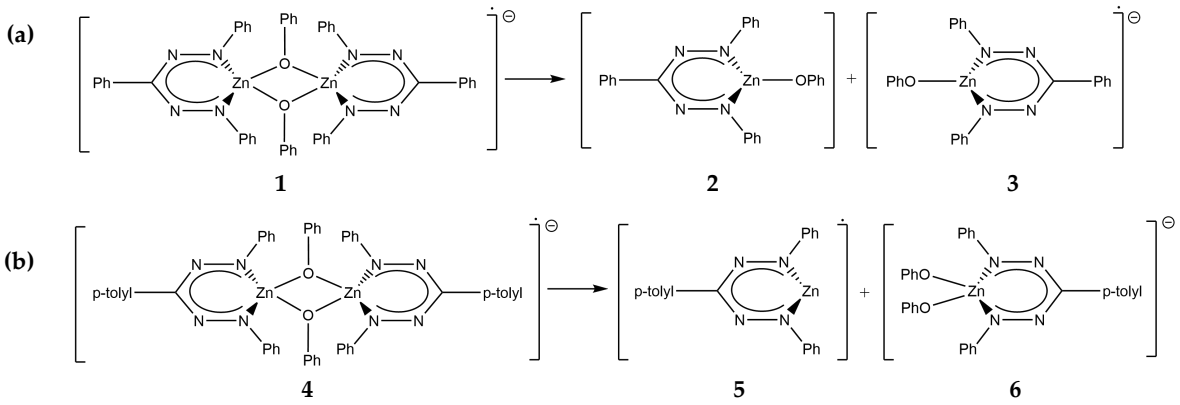

Scheme 4.1 The formations of formazanate zinc complexes. The complexes **2** and **3** in **(a)** are used for pathway A and pathway B, and the complex **5** in **(b)** is used for the pathway C.

The formations of mono(formazanate)zinc complexes are shown in *Scheme 4.1(a)* and *(b)*. The neutral (**2**), radical anionic (**3**) and radical (**5**) mono(formazanate)zinc complexes can be obtained by asymmetric dissociation of the zinc dimers. The backbone of complex **3** has a low-lying empty orbitals capable of accepting electrons (*Figure 4.1*)[35]. Therefore, it is expected that *Scheme 4.1(a)* requires a lower energy as it produces complex **3**.

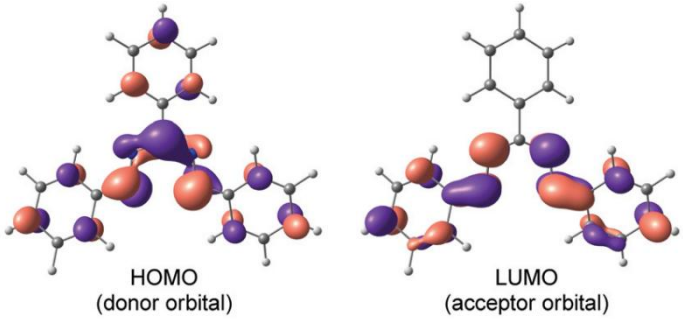

Figure 4.1 The HOMO and LUMO of 'closed' formazanate ligand[35].

According to *Scheme 4.1(a)* and *(b)*, the dissociation energy for the formation of neutral complex **2** and radical anionic complex **3** from the zinc dimer **1** is 21.6 kcal/mol, and for the formation of complex **5** and complex 6 from zinc dimer **4** is 37.4 kcal/mol (*Table 4.1*). Complexes **2** and **3** are the active species in pathways A and B, respectively. Complex **5** has two sites capable of coordinating with lactate, so it is the active species of pathway C.

The mechanisms of all three pathways have been calculated to see if they all carried out the ROP of lactide with relatively low Gibbs free energy changes. In pathways A and B, the substituent *R* group attached to C^3 in the formazanate NNCNN backbone is the Ph group in order to reduce the computational cost; whereas in pathway C, it is the *p*-tolyl group for consistency with the experiment[52]. Since the Ph and *p*-tolyl groups are aryl groups, the formazanate backbone is in a 'closed' (*trans-syn*, s-*cis*) conformation in both cases[35]. The aryl substituents contribute to the HOMO and LUMO of the formazanate ligands: the π-conjugated systems among Ar^1, Ar^5 and *R* group contributes to HOMO through resonance effect, while $Ar^1$and Ar^5 contribute to LUMO through resonance effect, but the *R* group through inductive effect as it owns a nodal plane (*Figure 4.1*)[35].

The energy for the dissociation of zinc dimers and the coordination of lactide to active species in three pathways are shown in *Table 4.1*. This result suggests that complex **3** is more favourable than complex **2** when one site is available for coordinating lactide, while the postulate that complex **5** coordinates with two lactides appears to be more favourable from an energetic point of view than the former case when two sites are available.

Table 4.1 Dissociation energies (ΔD) and the binding energies of lactide to active species (ΔG_B).

Pathway	$1 \rightarrow 2 + 3$	$4 \rightarrow 5 + 6$		A	B	C
ΔD (kcal/mol)	21.6	37.4	ΔG_B (kcal/mol)	4.5	4.0	−0.4

4.2 Pathways A and B: Insertion of the first the lactide monomer

Pathways A and B have the same mechanism but use different active species. The active species is complex **2** for pathway A and complex **3** for pathway B. The differences in the energy diagrams show the effect of using neutral (**2**) or radical anionic (**3**) complexes on the energy of each state of this mechanism and the activation energy of this reaction. As the mechanisms are the same, only the schemes for pathway B are given in the following.

The reaction starts with the coordination complex [Zn]−LA, where the O−Ph group and the lactide each occupy both sides of the formazanate plane. The energy diagrams of pathways A and B are shown in *Figure 4.2*. Compared to the neutral complex **2**, the radical anionic complex **3** requires more energy to process this ROP.

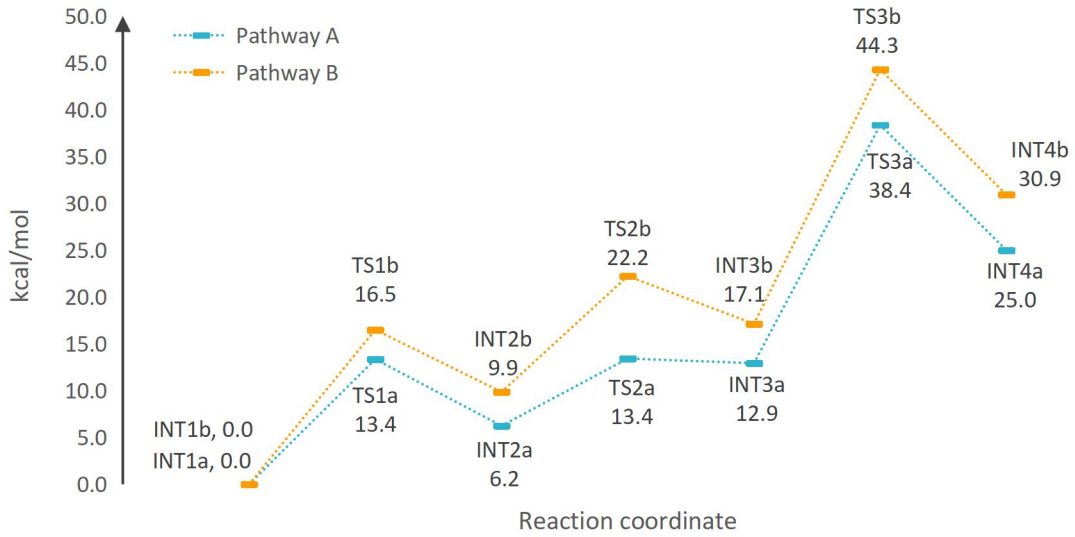

Figure 4.2 The energy diagram of pathway A and pathway B.

Scheme 4.2 shows the insertion of the first lactide into Zn(II) complex. When the O−Ph group and lactide are almost parallel, the O atom of O−Ph undergoes nucleophilic attack on the carbonyl carbon of lactide. The distance between O and C when it occurs is 1.80 Å. As shown in *Figure 4.1*, the E_a for this step of pathways A and B are 13.4 and 16.5 kcal/mol respectively. Intermediate **INT2b** shows the structure of the compound after insertion of lactide, where OPh group is attached to the carbon in the previous carbonyl group rather than coordinated to the zinc atom.

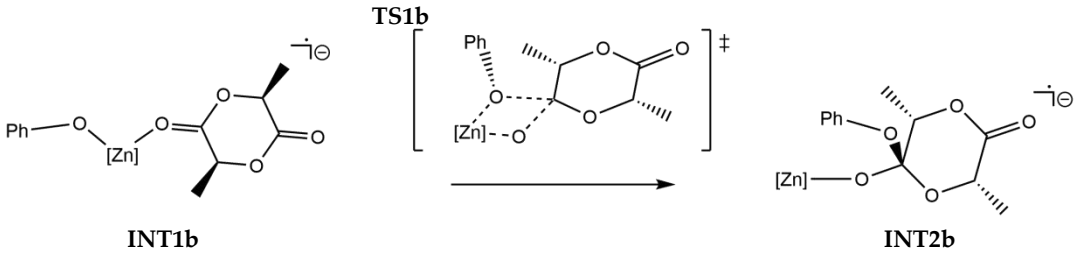

Scheme 4.2 The insertion of the first lactide.

When the O next to the C of the previous carbonyl group, namely $O_{\alpha 1}$, is coordinated to the zinc atom, the C−$O_{\alpha 1}$ bond of lactide breaks, leading to the opening of the lactide ring, as shown in *Scheme 4.3*. As shown in *Figure 4.2*, the E_a are 13.4 and 22.2 kcal/mol for the pathways A and B, respectively. However, the insertion of the first lactide is energetically unfavourable as the Gibbs free energy change (ΔG) is positive for both pathways A and B; they require energies of 12.9 and 17.1 kcal/mol, respectively.

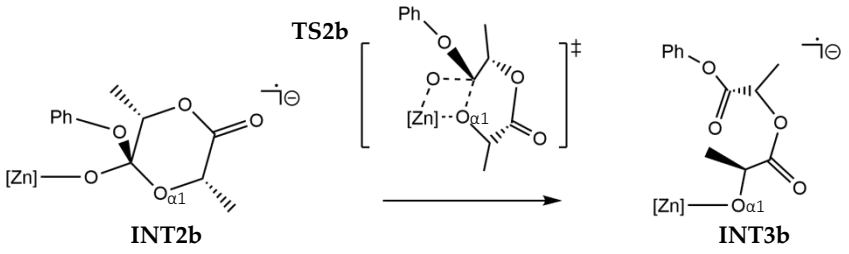

Scheme 4.3 The ring-opening of the first lactide.

4.3 Pathways A and B: Insertion of the second lactide monomer

Scheme 4.4 shows the insertion of the second lactide, which begins with the nucleophilic attack of the $O_{\alpha 1}$ next to the zinc atom on the carbonyl carbon of the second lactide. In pathway A, the E_a of the $O_{\alpha 1}$→C attack is 25.5 kcal/mol with respect to **INT3a** and 38.4 kcal/mol with respect to **INT1a**. The energy decreases rapidly after the insertion and the energy difference between **INT3a** and **INT4a** is 12.1 kcal/mol. Pathway B shows a similar trend, with E_a for the $O_{\alpha 1}$→C attack being 27.2 kcal/mol relative to **INT3b**, 44.3 kcal/mol relative to **INT1b**, and an energy difference of 13.8 kcal/mol between **INT3b** and **INT4b**. Thus, the total energy rises even more after the addition of the second lactide. Although complexes **2** and **3** are favourable products of dissociation of zinc dimer **1**, the following ROPs are unlikely to occur.

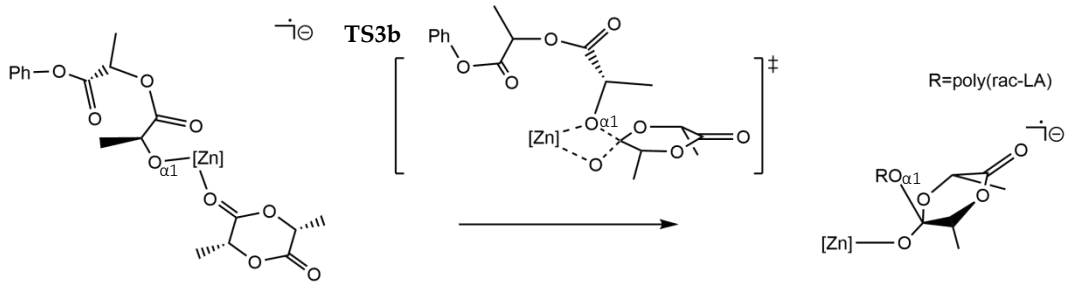

INT3b **INT4b**

Scheme 4.4 Insertion of the second lactide.

Table 4.2 shows the displacements of the zinc atom out of the formazanate plane at each state. The zinc atom behaves similarly when it carries a β-diketiminate ligand[14,42]. The increase in $d_{Zn\text{-}cat}$ indicates a higher level of steric crowding[14], especially when the first lactide opens the ring (i.e. **TS2a/b**). However, when the system is at **TS3b**, $d_{Zn\text{-}cat}$ is almost zero, indicating that the zinc atom returns to the plane. The $d_{Zn\text{-}cat}$ of **TS3a** (0.27 Å) is 10 times larger than that of **TS3b** (0.02 Å), therefore at **TS3b** the surrounding of the zinc atom is not as crowded as being at **TS3a**, or the zinc atom may be pushed back into the plane as the polymer chain occupies the space around the zinc atom.

Table 4.2 The zinc displacement $d_{Zn\text{-}cat}$(Å) of each state.

	INT1a/b	TS1a/b	INT2a/b	TS2a/b	INT3a/b	TS3a/b	INT4a/b
Pathway A	0.04	0.61	0.44	1.19	0.25	0.27	0.23
Pathway B	0.20	0.27	0.35	0.63	0.29	0.02	0.20

4.4 Pathway C

When two lactides coordinate to complex **5**, i.e. **5** + 2LA → **INT1c**, it has the Gibbs free energy difference of −0.4 kcal/mol. These two lactides, named LA^1 and LA^2, are able to coordinate with the zinc atom as there are two available sites.

Once the distance between the carbonyl carbon of LA^1 and a nitrogen atom next to the zinc atom is about 1.6 Å, the nitrogen atom can nucleophilic attack the carbonyl carbon, as shown in *Scheme 4.5(a)*. The zinc atom moves upward to make room for the coordination of LA^2. Due to the insertion of LA^1, the Ph group attached to the nitrogen atom undergoing nucleophilic attack is no longer in the formazanate plane, but turns

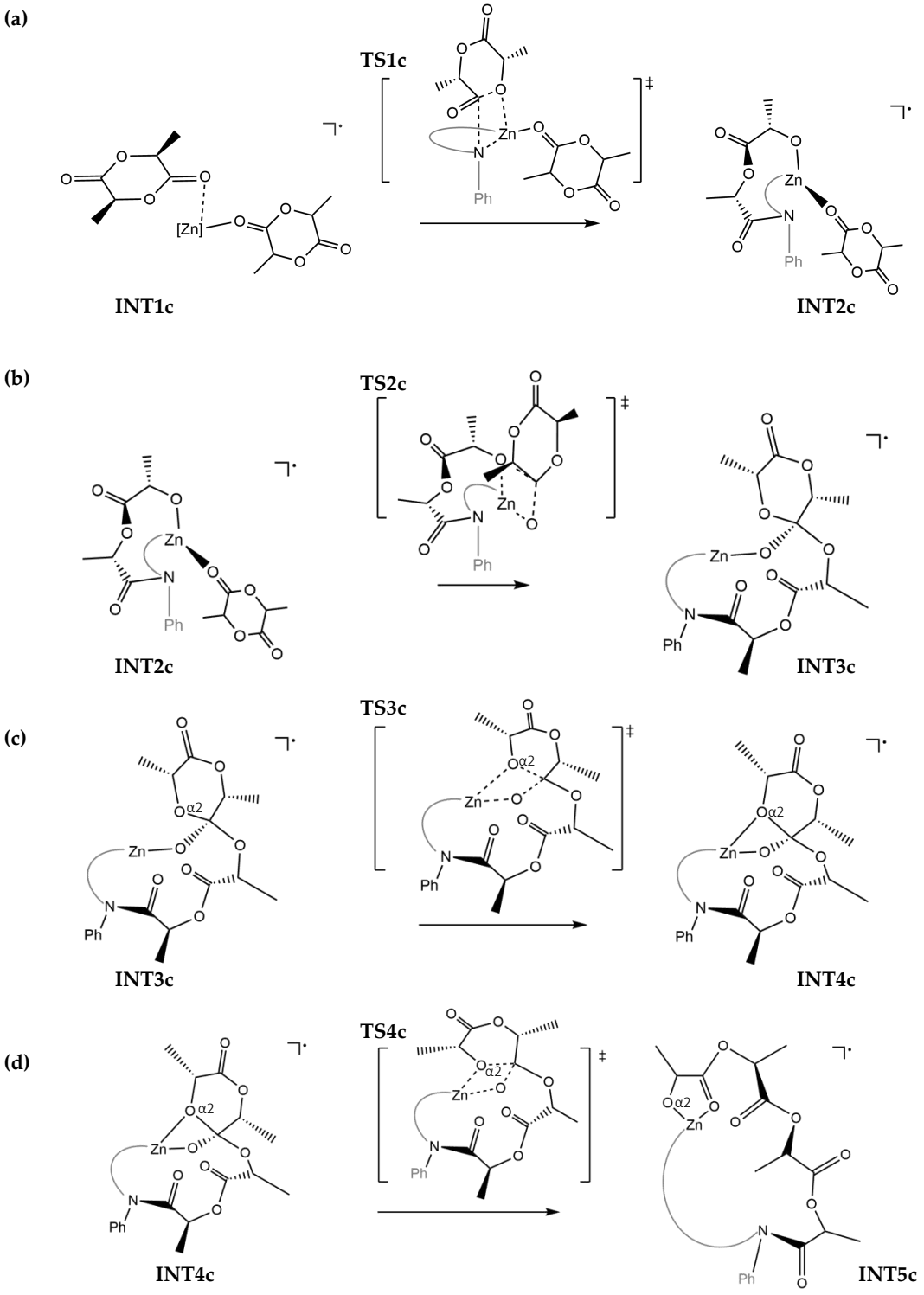

Scheme 4.5 (a) The nucleophilic attack of the nitrogen atom on carbonyl carbon; (b) the insertion of the second lactide; (c) the change in coordination; (d) the ring-opening of the second lactide.

towards to the other side not occupied by LA^1. As soon as the Zn−O coordination and N−C bond are established, the ring of LA^1 breaks. In short, the N→C nucleophilic attack is simultaneous with the ring-opening of LA^1.

When the distance between the oxygen atom next to the zinc and the carbonyl carbon of LA^2 is about 1.8 Å, the oxygen atom will undergo nucleophilic attack on carbonyl carbon, leading to the insertion of LA^2, as shown in *Scheme 4.5(b)*. This leads to the expansion of the cPLA chain created by the ring-opening of LA^1, which is displaced from zinc to make room for the ring-opening of LA^2.

Upon insertion, the oxygen next to the carbonyl carbon, $O_{\alpha 2}$, will coordinate to the zinc atom as indicated in *Scheme 4.5(c)*, resulting in a change in the coordination number of Zn. The carbonyl oxygen remains coordinated to the zinc atom, with a bond length of 1.9 Å for [Zn]−OC. The bond length of [Zn]−$O_{\alpha 2}$ is slightly longer, with a value of 2.1 Å. The bond between $O_{\alpha 2}$ and the carbonyl carbon of LA^2, C−$O_{\alpha 2}$, breaks at a distance between them of more than 1.8 Å, as shown in *Scheme 5.5(d)*. It results in a cPLA accompanied by isomerization of the formazanate backbone from a 'closed' (*trans-syn*, *s- cis*) to an 'open' (*trans-syn*, *s-trans*) geometry. The 'open' formazanate backbone favors the formation of a five-membered ring around the zinc atom at one end of the cPLA.

The energy diagram of this pathway is shown in *Figure 4.3*. The activation energy of each elementary step is shown in *Table 4.3*. The Gibbs free energy change of the pathway C is 5.0 kcal/mol, and the rate-determining step is **TS3c**, with ΔG of 25.8 kcal/mol. In contrast to pathways A and B, when the Zn(II) complex provides two available sites and the catalyst is a radical, the insertion of two lactides into the system requires less energy

Table 4.3 The activation energy E_a of each elementary step.

	TS1c	TS2c	TS3c	TS4c
E_a (kcal/mol)	18.8	12.4	9.3	1.5

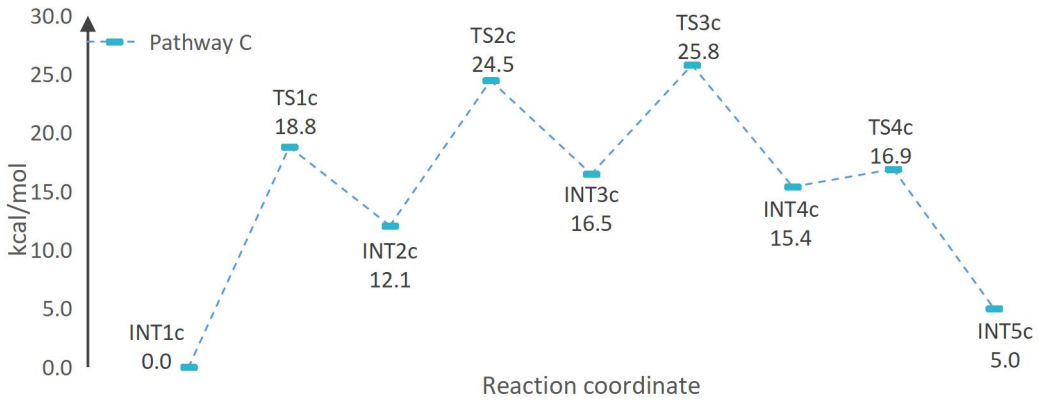

Figure 4.3 The energy diagram of the alternative pathway.

input. The activation energy E_{a1} required for **TS1c** is 18.8 kcal/mol, which stands for the nucleophilic attack of the N next to the zinc atom on the C of LA^1, accompanied by the ring-opening of LA^1. Starting with **INT2c**, the nucleophilic attack of the O next to the zinc atom in LA^1 on the carbonyl carbon in LA^2 needs the E_{a2} of 12.4 kcal/mol. The change in coordination number requires the E_{a3} of 9.3 kcal/mol with respect to **INT3c**. The ring-opening of LA^2 needs an E_{a4} of 1.5 kcal/mol. Finally, the ΔG of **INT5c** relative to **INT1c** is 5.0 kcal/mol.

4.5 Differences between the mechanisms of pathways A/B and C

According to *Figure 4.2*, the ΔG for pathways A and B continues to increase and shows no tendency to become lower. Though pathway C gives a positive ΔG for polymerizing two lactides, the addition of LA^2, i.e. from **INT2c** to **INT5c**, results in a change in ΔG of -7.1 kcal/mol, then the insertion of LA^3 is likely to be able to induce a negative ΔG. The most important differences between these two mechanisms are: 1) the amount of lactide bound by the active species when the system is at **INT1a/b/c**; 2) the PLA obtained by pathways A and B is linear, whereas pathway C is cyclic; and 3) the active species in pathway C changes its structure at **INT5c**, whereas the active species in pathways A and B maintain their original structures. Thus, the breakage of the Zn−N bond in the formazanate ligand allows the ligand to be more flexible so that steric hindrance can be released and then the state energy can be reduced, which then reduces the state energy of **INT5c**, resulting in a lower ΔG for pathway C than for pathways A and B.

Although the dissociation energy ΔD of zinc dimer **4** is higher than that of zinc dimer **1**, the subsequent reactions suggest that pathways A and B are impossible but pathway C is a feasible one. Further studies could focus on other ways of dissociation of the zinc dimer or to see if complex **5** can be obtained by the dissociation of complex **3**.

4.6 Comparison with other computational calculations

The ROPs of lactide using other metal complexes, such as magnesium and tin complexes, were investigated using the B3-LYP density functional procedure[41]. The structures of the β-diketiminate Mg(II) and Sn(II) complexes are shown in *Figure 4.4(a)* and *(b)*. Since the

(a) **(b)**

Figure 4.4 Structures of the metal catalysts: (a) the β-diketiminate Mg(II) complex[39]; (b) the β-diketiminate Sn(II) complex[42].

functionals and basis sets used to simulate the ROP of lactide with β-diketiminate Mg(II) and Sn(II) complexes are different from those applied to the ROP with formazanate Zn(II) complex, the value of activation energy E_a is used as a rough reference value to see if the formazanate zinc complex significantly lower the activation barrier. The value of ΔG is used to determine whether the mechanism using formazanate Zn(II) complex is feasible, and whether the ΔG given by pathway C is within a reasonable error range.

The mechanism used in the studies of the β-diketiminate Mg(II) and Sn(II) complexes is the coordination-insertion mechanism, and their **TS1** and **TS2** are similar to **TS1a/b** and **TS2a/b** in this study. **TS1** represents the state in which the metal atom coordinates the lactide and **TS2** refers to the ring-opening of the lactide. The E_a is 12.5 kcal/mol for **TS1** and 28.1 kcal/mol for **TS2** when the Mg(II) complex is used, while the E_a is 29.4 kcal/mol for **TS1** and 23.8 kcal/mol for **TS2** when the Sn(II) complex is used. **TS1a** and **TS2a** have the same value for E_a, which is 13.4 kcal/mol. From the data, it is highly likely that the formazanate Zn(II) complex can reduce the E_a used for the ring-opening step.

The ΔG for the ROP of two lactides with the Mg(II) complex is 3.7 kcal/mol; in the case of using the Sn(II) complex, the ΔG is -7.9 kcal/mol. Therefore, the effect of the calculation error on ΔG is likely to cause a positive ΔG for pathway C.

In the absence of a catalyst, the value of ΔG for the disruption of the ring structure of lactide using the $MeO^{\ominus}$ group is 1.3 kcal/mol. The enthalpy difference ΔH for it is -9.5 kcal/mol. When the temperature increase to 423.15 K, the ΔG is 10.7 kcal/mol and the ΔH is -4.3 kcal/mol. This supports to the suggestion that the error in calculation is likely to result in a positive ΔG given by pathway C. Errors may arise from the overestimated entropy or underestimated enthalpy of the simulated system. As the DFT method reports a negative ΔG from **INT2c** to **INT5c**, the insertion of LA^2 into the polymer chain is exothermic. Therefore, after polymerizing more lactides, ΔG is likely to decrease and then the total reaction has a negative ΔG.

4.7 Comparison with the β-diketiminate zinc complex

According to the investigations done by Chellali *et al.*[14], at a ratio of [LA]/[Zn]=250, by calculating the slope of the Semilogarithmic plots of conversion versus time, the rate for the ROP with the β-diketiminate Zn(II) catalyst is 0.013 s^{-1}. From **INT2c** to **INT3c** is an elementary step representing the insertion of LA^2, and has rate constant of approximately 0.03 s^{-1}. The state energy reported by the DFT method gives a fair approximation for the change from $(rac\text{-LA})_n$ to $(rac\text{-LA})_{n+1}$.

4.8 Comparison between the DFT and DFTB results

The evaluation of the accuracy of the DFTB method in predicting the pathway C is based on its calculated bond distances and state energies. The bond distances for N−C, N−N, N=C and N=N bonds are close to those given by the DFT method, but the N−N bond distance for **TS1c**, **TS2c**, **TS3c** and **TS4c** are slightly shorter than those given by the DFT method (*Table 4.4*). The N−N bond is linked to one end of *rac*-LA[1], so both methods give longer N − N bond distances and the DFTB method underestimates the N − N bond distance in an acceptable region. In general, the DFTB method gives reliable predictions on the changes in bond distance as the accuracy is ±0.01 Å.

Table 4.4 The bond distances (Å) of C−N, N−N, C=N and N=N given by DFTB and DFT methods.

	DFTB				DFT			
	TS1c'	TS2c'	TS3c'	TS4c'	TS1c	TS2c	TS3c	TS4c
C−N	1.37	1.37	1.37	1.37	1.36	1.36	1.36	1.36
N−N	1.40	**1.41**	**1.41**	**1.41**	1.39	**1.45**	**1.44**	**1.44**
C=N	1.35	1.34	1.33	1.33	1.33	1.32	1.32	1.33
N=N	1.33	1.33	1.33	1.33	1.33	1.33	1.33	1.33

The energy diagrams of the results given by DFTB and DFT methods are shown in *Figure 4.5*. The overestimation of the free energies by the DFTB method may be due to the fact that the system is less ordered than materials with periodic band structure. The presence of a delocalized system in the ligand may be another reason, since the interaction of the on-site charges is described after artificial stabilization[51]. The DFTB method gives much higher free energy for **INT5c**, may be due to a change in the geometry of the formazanate backbone, which changes its configuration from 'closed' to 'open', thus having a strong influence on the electron density distribution of the system. As the energy trend given by DFTB is very different from that given by DFT, in particular it gives almost the same free energy for TS1c and TS2c, it is not sufficient to predict the free energy change for the polymerization of cPLA, or DFTB is less accurate when operating on non-linear systems.

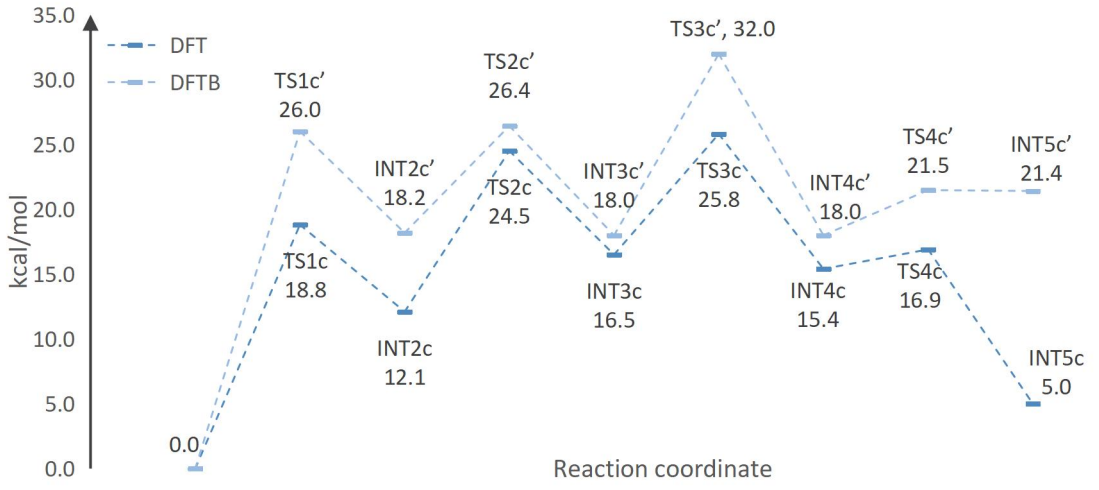

Figure 4.5 The energy diagrams of the results given by DFTB and DFT methods.

Chapter 5 Conclusions

This research described three types of ring-opening polymerization (ROP) using Zn(II) formazanate catalysts for the synthesis of cyclic polylactic acid (cPLA), namely pathways A, B and C. Key parameters, including bond distance and zinc displacement (Zn—d_{cat}), are obtained from the calculations. The calculation achieves the aim of finding active species and energetically favourable pathways. The active species are neutral complex **2**, radical anionic complex **3** and radical complex **5**. The results show that pathway C is the most feasible one among the three, with an activation energy of 18.8 kcal/mol for its rate-determining step. Its energy trend indicates that the reaction may be exothermic after a series of polymerization. When performing the coordination-insertion mechanism, the formazanate Zn(II) complex reduces the activation energy required for ring-opening of the lactide. The rate constant for the elementary step of inserting another lactide is 0.03 s^{-1} which is higher than that derived from data from experiments using structurally similar β-diketiminate zinc complex, suggesting that ROP with formazanate zinc complex can be completed more quickly.

The formazanate ligands provide a new research direction for the synthesis of cyclic PLA (cPLA). The mechanism revels that short polymer chain is linked to zinc atom at the chain end, indicating that pathway C probably produce cPLA. In contrast to Density Functional Theory (DFT) method, the Density-Functional based Tight-Binding (DFTB) method do not predict state energies sufficiently well, but can predict bond distances adequately. Thus, for the purposes of giving accurate state energies, the DFTB method cannot completely replace the DFT method.

No subsequent polymerization was performed in this study, which may account for the positive free energy change in pathway C, although it is closer to zero than in pathways A and B. The use of asymmetric formazanate ligand to simulate the reactions in order to reduce the activation energy of dissociation of dimeric zinc complex and the Gibbs free energy of the rate-determining step is a research direction that could be explored.

In summary, the radical anionic formazanate Zn(II) complex is capable of coordinating two monomers and performing ROP by a mechanism similar to coordination-insertion mechanism. Overall, three synthetic pathways have been successfully modelled in this study and pathway C provides a possible direction for the synthesis of PLA, partially contributing to the solution of plastic pollution.

Acknowledges

First and foremost, I would like to express my sincerest gratitude to my first supervisor, Prof. Dr. Remco Havenith, for his enlightening inspiration, thoughtful guidance and gentle encouragement throughout my Master's project. Without his patience and invaluable experience, the course of researching this project could not have been accompanied by a sense of joy and achievement. Also, many thanks to Prof. Dr. Edwin Otten for his ideas and feedbacks on this project.

I am also grateful to the other group members who shared their experiences and insights in writing the thesis. Moreover, thanks to the Erasmus Mundus Joint Masters programme, which gave me the opportunity to join the Theoretical Chemistry and Computational Modelling project and explore the field of theoretical chemistry.

Finally, I would like to express my appreciation to my parents for their endless love and the support, which has gave me the confidence and courage to overcome the difficulties I have faced during my Master's study.

Bibliography

[1] Rezvani Ghomi, E., Khosravi, F., Saedi Ardahaei, A., Dai, Y., Neisiany, R., Foroughi, F., Wu, M., Das, O. and Ramakrishna, S., 2021. The Life Cycle Assessment for Polylactic Acid (PLA) to Make It a Low-Carbon Material. Polymers, 13(11), p.1854.

[2] Benavides, P., Lee, U. and Zarè-Mehrjerdi, O., 2020. Life cycle greenhouse gas emissions and energy use of polylactic acid, bio-derived polyethylene, and fossil-derived polyethylene. Journal of Cleaner Production, 277, p.124010.

[3] Sharma, A., Singh, S., Khare, S., Sharma, A., Tiwari, R. and Nain, L., 2022. Green lactic acid production using low-cost renewable sources and potential applications. Production of Top 12 Biochemicals Selected by USDOE from Renewable Resources, pp.345-365.

[4] Char, J., Brulé, E., Gros, P., Rager, M., Guérineau, V. and Thomas, C., 2022. Synthesis of heterotactic PLA from rac-lactide using hetero-bimetallic Mg/Zn–Li systems.

[5] Athar, T., Hakeem, A. and Topnani, N., 2011. Synthesis of β-diketiminate derivatives of zinc alkoxides: catalytic properties for ring opening polymerization. Journal of the Chilean Chemical Society, 56(4), pp.887-890.

[6] Mehmood, A., Raina, N., Phakeenuya, V., Wonganu, B. and Cheenkachorn, K., 2022. The current status and market trend of polylactic acid as biopolymer: Awareness and needs for sustainable development. Materials Today: Proceedings,.

[7] Robert, C., Schmid, T., Richard, V., Haquette, P., Raman, S., Rager, M., Gauvin, R., Morin, Y., Trivelli, X., Guérineau, V., del Rosal, I., Maron, L. and Thomas, C., 2017. Mechanistic Aspects of the Polymerization of Lactide Using a Highly Efficient Aluminum(III) Catalytic System. Journal of the American Chemical Society, 139(17), pp.6217-6225.

[8] DeStefano, V., Khan, S. and Tabada, A., 2020. Applications of PLA in modern medicine. Engineered Regeneration, 1, pp.76-87.

[9] Carothers, W. H., Dorough, G. L., & Natta, F. V. (1932). Studies of polymerization and ring formation. X. The reversible polymerization of six-membered cyclic esters. Journal of the American Chemical Society, 54(2), 761-772.

[10] Darensbourg, D., Choi, W., Karroonnirun, O. and Bhuvanesh, N., 2008. Ring-Opening Polymerization of Cyclic Monomers by Complexes Derived from Biocompatible Metals. Production of Poly(lactide), Poly(trimethylene carbonate), and Their Copolymers. Macromolecules, 41(10), pp.3493-3502.

[11] Moon SI, Lee CW, Miyamoto M, Kimura Y. Melt polycondensation of l-lactic acid with Sn(II) catalysts activated by various proton acids: a direct manufacturing route to high molecular weight poly(l-lactic acid). J Polym Sci, Part A: Polym Chem 2000;38:1673–9

[12] Maharana, T., Mohanty, B. and Negi, Y.S. (2009) "Melt–solid polycondensation of lactic acid and its biodegradability," *Progress in Polymer Science*, 34(1), pp. 99–124. Available at: https://doi.org/10.1016/j.progpolymsci.2008.10.001.

[13] Drouin, F., Oguadinma, P., Whitehorne, T., Prud'homme, R. and Schaper, F., 2010. Lactide Polymerization with Chiral β-Diketiminate Zinc Complexes. Organometallics, 29(9), pp.2139-2147.

[14] Chellali, J., Alverson, A. and Robinson, J., 2022. Zinc Aryl/Alkyl β-diketiminates: Balancing Accessibility and Stability for High-Activity Ring-Opening Polymerization of rac-Lactide. ACS Catalysis, 12(9), pp.5585-5594.

[15] Chamberlain, B., Cheng, M., Moore, D., Ovitt, T., Lobkovsky, E. and Coates, G., 2001. Polymerization of Lactide with Zinc and Magnesium β-Diiminate Complexes: Stereocontrol and Mechanism. Journal of the American Chemical Society, 123(14), pp.3229-3238.

[16] Amgoune, A., Thomas, C., Roisnel, T. and Carpentier, J., 2006. Ring-Opening Polymerization of Lactide with Group 3 Metal Complexes Supported by Dianionic Alkoxy-Amino-Bisphenolate Ligands: Combining High Activity, Productivity, and Selectivity. Chemistry - A European Journal, 12(1), pp.169-179.

[17] Chisholm, M., Gallucci, J. and Phomphrai, K., 2005. Comparative Study of the Coordination Chemistry and Lactide Polymerization of

Alkoxide and Amide Complexes of Zinc and Magnesium with a β-Diiminato Ligand Bearing Ether Substituents. Inorganic Chemistry, 44(22), pp.8004-8010.

[18] Dove, A.P. (2008) “Controlled ring-opening polymerisation of cyclic esters: Polymer blocks in self-assembled nanostructures,” *Chemical Communications*, (48), p. 6446. Available at: https://doi.org/10.1039/b813059k.

[19] Zecchina, A., Bordiga, S. and Groppo, E., 2011. Selective nanocatalysts and nanoscience. Weinheim: Wiley-VCH.

[20] Byers, J.A., Biernesser, A.B., Delle Chiaie, K.R., Kaur, A., Kehl, J.A. (2017). Catalytic Systems for the Production of Poly(lactic acid). In: Di Lorenzo, M., Androsch, R. (eds) Synthesis, Structure and Properties of Poly(lactic acid). Advances in Polymer Science, vol 279. Springer, Cham. https://doi.org/10.1007/12_2017_20

[21] Baseden, K. and Tye, J., 2014. Introduction to Density Functional Theory: Calculations by Hand on the Helium Atom. Journal of Chemical Education, 91(12), pp.2116-2123.

[22] Atkins, P.W. and Friedman, R. (2011) *Molecular quantum mechanics*. Oxford: Oxford University Press.

[23] Born, M. and Oppenheimer, R. (1927), Zur Quantentheorie der Molekeln. Ann. Phys., 389: 457-484. https://doi.org/10.1002/andp.19273892002

[24] Koch, W. and Holthausen, M., 2001. A Chemist's Guide to Density Functional Theory.

[25] Perdew, J., Burke, K. and Ernzerhof, M., 1996. Generalized Gradient Approximation Made Simple. Physical Review Letters, 77(18), pp.3865-3868.

[26] Yu, P.Y. and Cardona, M. (2010) *Fundamentals of Semiconductors: Physics and Materials Properties*. New York: Springer.

[27] Vukmirović, N. and Wang, L., 2011. Quantum Dots: Theory. Comprehensive Nanoscience and Technology, pp.189-217.

[28] Lima, G., Heine, T. and Duarte, H., 2010. Molecular Dynamics of Polypeptides and Their Inclusion Compounds with β-Cyclodextrin in Aqueous Solution Using DC–SCC–DFTB/UFF Approach. Advances in Quantum Chemistry, pp.145-180.

[29] Gaus, M., Cui, Q. and Elstner, M., 2011. DFTB3: Extension of the Self-Consistent-Charge Density-Functional Tight-Binding Method (SCC-DFTB). Journal of Chemical Theory and Computation, 7(4), pp.931-948.

[30] van Lenthe, E., Snijders, J. G., & Baerends, E. J. (1996). The zero-order regular approximation for relativistic effects: The effect of spin-orbit coupling in closed shell molecules. Journal of Chemical Physics, 105(15), 6505 - 6516. https://doi.org/10.1063/1.472460

[31] Dennis, J. E., & Jorge J. Morée. (1977). Quasi-Newton Methods, Motivation and Theory. SIAM Review, 19(1), 46–89. http://www.jstor.org/stable/2029325

[32] Dove, A.P. (2008) “Controlled ring-opening polymerisation of cyclic esters: Polymer blocks in self-assembled nanostructures,” Chemical Communications, (48), p. 6446. Available at: https://doi.org/10.1039/b813059k.

[33] AMS Driver Manual 2022.1 (2022) Software for Chemistry & Materials. Available at: https://www.scm.com/doc/AMS/index.html (Accessed: October 23, 2022).

[34] Itoh, S. and Morimoto, Y. (2015) “B-diketiminates as redox non-innocent supporting ligands in coordination chemistry,” Chemical Science of π-Electron Systems, pp. 715–730. Available at: https://doi.org/10.1007/978-4-431-55357-1_42.

[35] Gilroy, J.B. and Otten, E. (2020) “Formazanate coordination compounds: Synthesis, reactivity, and applications,” Chemical Society Reviews, 49(1), pp. 85–113. Available at: https://doi.org/10.1039/c9cs00676a.

[36] Kricheldorf, H.R., Kreiser-Saunders, I., Jürgens, C. and Wolter, D. (1996), Polylactides - synthesis, characterization and medical application. Macromol. Symp., 103: 85-102. https://doi.org/10.1002/masy.19961030110

[37] Hopkinson, M., Richter, C., Schedler, M. and Glorius, F., 2014. An overview of N-heterocyclic carbenes. Nature, 510(7506), pp.485-496.

[38] Tsuzuki, S., Honda, K., Uchimaru, T., Mikami, M. and Tanabe, K., 2001. Origin of Attraction and Directionality of the π/π Interaction: Model Chemistry Calculations of Benzene Dimer Interaction. Journal of the American Chemical Society, 124(1), pp.104-112.

[39] Marshall, E.L., Gibson, V.C. and Rzepa, H.S. (2005) "A computational analysis of the ring-opening polymerization of rac-lactide initiated by single-site β-diketiminate metal complexes: defining the mechanistic pathway and the origin of stereocontrol," *Journal of the American Chemical Society*, 127(16), pp. 6048 – 6051. Available at: https://doi.org/10.1021/ja043819b.

[40] Duda, A. and Penczek, S. (1990) "Thermodynamics of L-lactide polymerization. equilibrium monomer concentration," *Macromolecules*, 23(6), pp. 1636 – 1639. Available at: https://doi.org/10.1021/ma00208a012.

[41] Nifant'ev, I. and Ivchenko, P. (2019) "Coordination ring-opening polymerization of cyclic esters: A critical overview of DFT modeling and visualization of the reaction mechanisms," *Molecules*, 24(22), p. 4117. Available at: https://doi.org/10.3390/molecules24224117.

[42] Dove, A.P. et al. (2006) "Synthetic, structural, mechanistic, and computational studies on single-site β-diketiminate tin(ii) initiators for the polymerization of rac-lactide," Journal of the American Chemical Society, 128(30), pp. 9834–9843. Available at: https://doi.org/10.1021/ja061400a.

[43] D'Alterio, M.C. et al. (2022) "Are well performing catalysts for the ring opening polymerization of l-lactide under mild laboratory conditions suitable for the industrial process? the case of new highly active zn(ii) catalysts," *Macromolecules*, 55(12), pp. 5115 – 5122. Available at: https://doi.org/10.1021/acs.macromol.2c00719.

[44] Hu, C. et al. (2017) "Cyclic versus linear polylactide: Straightforward access using a single catalyst," *Journal of Polymer Science Part A: Polymer Chemistry*, 55(19), pp. 3175–3179. Available at: https://doi.org/10.1002/pola.28699.

[45] Haque, F.M., Grayson, S.M. The synthesis, properties and potential applications of cyclic polymers. *Nat. Chem.* 12, 433–444 (2020). https://doi.org/10.1038/s41557-020-0440-5

[46] Semlyen, J.A. (1986) *Cyclic polymers*. London: Elsevier Applied Science Publ.

[47] Hoskins, J.N. and Grayson, S.M. (2009) "Synthesis and degradation behavior of cyclic poly(ε-caprolactone)," *Macromolecules*, 42(17), pp. 6406–6413. Available at: https://doi.org/10.1021/ma9011076.

[48] Zhu, Y. and Hosmane, N.S. (2015) "Advanced developments in cyclic polymers: Synthesis, applications, and perspectives," *ChemistryOpen*, 4(4), pp. 408–417. Available at: https://doi.org/10.1002/open.201402172.

[49] Chen, C. (2018) "Redox-controlled polymerization and Copolymerization," *ACS Catalysis*, 8(6), pp. 5506–5514. Available at: https://doi.org/10.1021/acscatal.8b01096.

[50] Gregson, C.K. et al. (2006) "Redox control within single-site polymerization catalysts," *Journal of the American Chemical Society*, 128(23), pp. 7410–7411. Available at: https://doi.org/10.1021/ja061398n.

[51] Lundberg, M., Nishimoto, Y. and Irle, S. (2012), Delocalization errors in a hubbard-like model: Consequences for density-functional tight-binding calculations of molecular systems. Int. J. Quantum Chem., 112: 1701-1711. https://doi.org/10.1002/qua.23178

[52] De Vries, F., & Otten, E. (2022). Reversible On/Off Switching of Lactide Cyclopolymerization with a RedoxActive Formazanate Ligand. ACS Catalysis, 12(7), 4125-4130. https://doi.org/10.1021/acscatal.1c05689

[53] Goonesinghe, C. et al. (2022) "An air stable cationic indium catalyst for formation of high-molecular-weight cyclic poly(lactic acid)," *ACS Catalysis*, 12(13), pp. 7677–7686. Available at: https://doi.org/10.1021/acscatal.2c02118.

[54] Jensen, F. (2017) *Introduction to computational chemistry.* Chichester, UK: Wiley.

[55] DeStefano, V., Khan, S. and Tabada, A., 2020. Applications of PLA in modern medicine. Engineered Regeneration, 1, pp.76-87.

[56] Hopkinson, M., Richter, C., Schedler, M. and Glorius, F., 2014. An overview of N-heterocyclic carbenes. Nature, 510(7506),

pp.485-496.

[57] Teixeira, S.; Eblagon, K.M.; Miranda, F.; R. Pereira, M.F.; Figueiredo, J.L. Towards Controlled Degradation of Poly(lactic) Acid in Technical Applications. C 2021, 7, 42. https://doi.org/10.3390/c7020042

[58] Kan, C., Hu, J., Huang, Y., Wang, H. and Ma, H., 2017. Highly Isoselective and Active Zinc Catalysts for rac-Lactide Polymerization: Effect of Pendant Groups of Aminophenolate Ligands. Macromolecules, 50(20), pp.7911-7919.

[59] Orhan, B., Tschan, M., Wirotius, A., Dove, A., Coulembier, O. and Taton, D., 2018. Isoselective Ring-Opening Polymerization of rac-Lactide from Chiral Takemoto's Organocatalysts: Elucidation of Stereocontrol. ACS Macro Letters, 7(12), pp.1413-1419.

[60] Dove, A., Gibson, V., Marshall, E., Rzepa, H., White, A. and Williams, D., 2006. Synthetic, Structural, Mechanistic, and Computational Studies on Single-Site β-Diketiminate Tin(II) Initiators for the Polymerization of rac-Lactide. Journal of the American Chemical Society, 128(30), pp.9834-9843.

[61] Zhong, Z., Schneiderbauer, S., Dijkstra, P.J. et al. Single-Site Calcium Initiators for the Controlled Ring-Opening Polymerization of Lactides and Lactones. Polymer Bulletin 51, 175–182 (2003). https://doi.org/10.1007/s00289-003-0211-7

[62] Ouchi, M., Terashima, T. and Sawamoto, M., 2009. Transition Metal-Catalyzed Living Radical Polymerization: Toward Perfection in Catalysis and Precision Polymer Synthesis. Chemical Reviews, 109(11), pp.4963-5050.

[63] Zhong, M., Sinhababu, S. and Roesky, H., 2020. The unique β-diketiminate ligand in aluminum(i) and gallium(i) chemistry. Dalton Transactions, 49(5), pp.1351-1364.

[64] Cheng, M., Moore, D., Reczek, J., Chamberlain, B., Lobkovsky, E. and Coates, G., 2001. Single-Site β-Diiminate Zinc Catalysts for the Alternating Copolymerization of CO2 and Epoxides: Catalyst Synthesis and Unprecedented Polymerization Activity. Journal of the American Chemical Society, 123(36), pp.8738-8749.

[65] Zheng, H., Narkhede, N., Han, L., Zhang, H. and Li, Z., 2019. Methanol synthesis from CO2: a DFT investigation on Zn-promoted Cu catalyst. Research on Chemical Intermediates, 46(3), pp.1749-1769.

[66] Zecchina, A., Bordiga, S. and Groppo, E., 2011. Selective nanocatalysts and nanoscience. Weinheim: Wiley-VCH.

[67] Koch, W. and Holthausen, M., n.d. A Chemist's Guide to Density Functional Theory.

[68] Tokatly, I., Stubner, R. and Pankratov, O., 2002. Many-body diagrammatic expansion for the exchange-correlation kernel in time-dependent density functional theory. Physical Review B, 65(11).

[69] Lima, G., Heine, T. and Duarte, H., 2010. Molecular Dynamics of Polypeptides and Their Inclusion Compounds with β-Cyclodextrin in Aqueous Solution Using DC–SCC–DFTB/UFF Approach. Advances in Quantum Chemistry, pp.145-180.

[70] Foulkes, W. and Haydock, R., 1989. Tight-binding models and density-functional theory. Physical Review B, 39(17), pp.12520-12536.

[71] Seifert, G., 2007. Tight-Binding Density Functional Theory: An Approximate Kohn−Sham DFT Scheme. The Journal of Physical Chemistry A, 111(26), pp.5609-5613.

[72] Rojan P. John, G.S. Anisha, Nimisha R. Nair and K.M. Nampoothiri (2011) Polylactic acid: an environmentally friendly biopolymer, pp. 79-90, In: Biodegradable Materials: Production, Properties and Applications, Brandon M. Johnson and Zachary E. Berkel (Eds.), Materials Science and Technology Series, Nova Science Publishers, Inc. 400 Oser Avenue, Suite 1600 Hauppauge, NY 11788, ISBN: 978-1-61122-804-5

[73] Gallaway, J., McRae, J., Decken, A. and Shaver, M., 2012. Ring-opening polymerization of rac-lactide and ε-caprolactone using zinc and calcium salicylaldiminato complexes. Canadian Journal of Chemistry, 90(5), pp.419-426.

[74] Grévy, J., 2006. Zinc: Organometallic ChemistryBased in part on the article Zinc: Organometallic Chemistry by Gerard Parkin which appeared in theEncyclopedia of Inorganic Chemistry, First Edition. Encyclopedia of Inorganic Chemistry,.

[75] Kashyap, C., Ullah, S., Mazumder, L. and Kanti Guha, A., 2018. Non-covalent interaction in benzene and substituted benzene: A theoretical study. Computational and Theoretical Chemistry, 1130, pp.134-139.

[76] Balla, E., Daniilidis, V., Karlioti, G., Kalamas, T., Stefanidou, M., Bikiaris, N., Vlachopoulos, A., Koumentakou, I. and Bikiaris, D., 2021. Poly(lactic Acid): A Versatile Biobased Polymer for the Future with Multifunctional Properties—From Monomer Synthesis, Polymerization Techniques and Molecular Weight Increase to PLA Applications. Polymers, 13(11), p.1822.

[77] Itoh, S. and Morimoto, Y. (2015) “B-diketiminates as redox non-innocent supporting ligands in coordination chemistry,” Chemical Science of π-Electron Systems, pp. 715–730. Available at: https://doi.org/10.1007/978-4-431-55357-1_42.

Appendix

I. Dissociation energies of dimeric zinc complexes

State energy *E* (hartree)			**Δ*D* (hartree)**	**Δ*D* (kcal/mol)**
1	**2**	**3**		
-25.59329576	-12.10155127	-12.24491256	0.069109724	43.36635159
	4	**5**		
	-12.12661179	-12.25457759	0.034384178	21.57607141
6	**7**	**8**		
-25.59329576	-9.819442887	-15.71428982	0.059563044	37.37581019

II. Energies for formation of INT1a, INT1b and INT1c

Pathway	**Lactide (hartree)**	**Complex (hartree)**	**INT1 (hartree)**	**Δ*G* (hartree)**	**Δ*G* (kcal/mol)**
A	-3.988342558	-12.12661179	-16.10775784	0.007196508	4.515808753
B		-12.25457759	-16.23658598	0.006334165	3.974688651
C		-9.819442887	-17.79679415	-0.000666149	-0.418008491

III. Rate constants

			T (K)	298
			$\Delta G_{reactant}$ (kcal/mol)	5.0
	ΔG_{TS} (kcal/mol)	**$\Delta G_{TS} - \Delta G_{reactant}$ (kcal/mol)**	**$\Delta G_{TS} - \Delta G_{reactant}$ (kJ/mol)**	***k*** **(s^{-1})**
TS1c	18.8	13.8	57777.81499	463.2040592
TS2c	24.5	19.5	81642.56467	0.030392684
TS3c	25.8	20.8	87085.40231	0.003378709
TS4c	16.9	11.9	49822.89844	11484.35984

Where $\Delta G_{reactant}$ is the Gibbs free energy change of the overall reaction; ΔG_{TS} is the Gibbs free energy difference between a transition state and **INT1c**.